EUROPEAN ORGANIZATION FOR NUCLEAR RESEARCH

CERN-EP-2003-067
09 October 2003

Experimental studies of unbiased gluon jets from e^+e^- annihilations using the jet boost algorithm

The OPAL Collaboration

Abstract

We present the first experimental results based on the jet boost algorithm, a technique to select unbiased samples of gluon jets in e^+e^- annihilations, i.e. gluon jets free of biases introduced by event selection or jet finding criteria. Our results are derived from hadronic Z^0 decays observed with the OPAL detector at the LEP e^+e^- collider at CERN. First, we test the boost algorithm through studies with Herwig Monte Carlo events and find that it provides accurate measurements of the charged particle multiplicity distributions of unbiased gluon jets for jet energies larger than about 5 GeV, and of the jet particle energy spectra (fragmentation functions) for jet energies larger than about 14 GeV. Second, we apply the boost algorithm to our data to derive unbiased measurements of the gluon jet multiplicity distribution for energies between about 5 and 18 GeV, and of the gluon jet fragmentation function at 14 and 18 GeV. In conjunction with our earlier results at 40 GeV, we then test QCD calculations for the energy evolution of the distributions, specifically the mean and first two non-trivial normalized factorial moments of the multiplicity distribution, and the fragmentation function. The theoretical results are found to be in global agreement with the data, although the factorial moments are not well described for jet energies below about 14 GeV.

(Submitted to Phys. Rev. D)

The OPAL Collaboration

G. Abbiendi[2], C. Ainsley[5], P.F. Åkesson[3,y], G. Alexander[22], J. Allison[16], P. Amaral[9], G. Anagnostou[1], K.J. Anderson[9], S. Arcelli[2], S. Asai[23], D. Axen[27], G. Azuelos[18,a], I. Bailey[26], E. Barberio[8,p], T. Barillari[32], R.J. Barlow[16], R.J. Batley[5], P. Bechtle[25], T. Behnke[25], K.W. Bell[20], P.J. Bell[1], G. Bella[22], A. Bellerive[6], G. Benelli[4], S. Bethke[32], O. Biebel[31], O. Boeriu[10], P. Bock[11], M. Boutemeur[31], S. Braibant[8], L. Brigliadori[2], R.M. Brown[20], K. Buesser[25], H.J. Burckhart[8], S. Campana[4], R.K. Carnegie[6], B. Caron[28], A.A. Carter[13], J.R. Carter[5], C.Y. Chang[17], D.G. Charlton[1], C. Ciocca[2], A. Csilling[29], M. Cuffiani[2], S. Dado[21], A. De Roeck[8], E.A. De Wolf[8,s], K. Desch[25], B. Dienes[30], M. Donkers[6], J. Dubbert[31], E. Duchovni[24], G. Duckeck[31], I.P. Duerdoth[16], E. Etzion[22], F. Fabbri[2], L. Feld[10], P. Ferrari[8], F. Fiedler[31], I. Fleck[10], M. Ford[5], A. Frey[8], A. Fürtjes[8], P. Gagnon[12], J.W. Gary[4], G. Gaycken[25], C. Geich-Gimbel[3], G. Giacomelli[2], P. Giacomelli[2], M. Giunta[4], J. Goldberg[21], E. Gross[24], J. Grunhaus[22], M. Gruwé[8], P.O. Günther[3], A. Gupta[9], C. Hajdu[29], M. Hamann[25], G.G. Hanson[4], A. Harel[21], M. Hauschild[8], C.M. Hawkes[1], R. Hawkings[8], R.J. Hemingway[6], C. Hensel[25], G. Herten[10], R.D. Heuer[25], J.C. Hill[5], K. Hoffman[9], D. Horváth[29,c], P. Igo-Kemenes[11], K. Ishii[23], H. Jeremie[18], P. Jovanovic[1], T.R. Junk[6], N. Kanaya[26], J. Kanzaki[23,u], D. Karlen[26], K. Kawagoe[23], T. Kawamoto[23], R.K. Keeler[26], R.G. Kellogg[17], B.W. Kennedy[20], K. Klein[11,t], A. Klier[24], S. Kluth[32], T. Kobayashi[23], M. Kobel[3], S. Komamiya[23], L. Kormos[26], T. Krämer[25], P. Krieger[6,l], J. von Krogh[11], K. Kruger[8], T. Kuhl[25], M. Kupper[24], G.D. Lafferty[16], H. Landsman[21], D. Lanske[14], J.G. Layter[4], D. Lellouch[24], J. Letts[o], L. Levinson[24], J. Lillich[10], S.L. Lloyd[13], F.K. Loebinger[16], J. Lu[27,w], A. Ludwig[3], J. Ludwig[10], A. Macpherson[28,i], W. Mader[3], S. Marcellini[2], A.J. Martin[13], G. Masetti[2], T. Mashimo[23], P. Mättig[m], W.J. McDonald[28], J. McKenna[27], T.J. McMahon[1], R.A. McPherson[26], F. Meijers[8], W. Menges[25], F.S. Merritt[9], H. Mes[6,a], A. Michelini[2], S. Mihara[23], G. Mikenberg[24], D.J. Miller[15], S. Moed[21], W. Mohr[10], T. Mori[23], A. Mutter[10], K. Nagai[13], I. Nakamura[23,v], H. Nanjo[23], H.A. Neal[33], R. Nisius[32], S.W. O'Neale[1], A. Oh[8], A. Okpara[11], M.J. Oreglia[9], S. Orito[23,*], C. Pahl[32], G. Pásztor[4,g], J.R. Pater[16], J.E. Pilcher[9], J. Pinfold[28], D.E. Plane[8], B. Poli[2], J. Polok[8], O. Pooth[14], M. Przybycień[8,n], A. Quadt[3], K. Rabbertz[8,r], C. Rembser[8], P. Renkel[24], J.M. Roney[26], S. Rosati[3,y], Y. Rozen[21], K. Runge[10], K. Sachs[6], T. Saeki[23], E.K.G. Sarkisyan[8,j], A.D. Schaile[31], O. Schaile[31], P. Scharff-Hansen[8], J. Schieck[32], T. Schörner-Sadenius[8,a1], M. Schröder[8], M. Schumacher[3], C. Schwick[8], W.G. Scott[20], R. Seuster[14,f], T.G. Shears[8,h], B.C. Shen[4], P. Sherwood[15], A. Skuja[17], A.M. Smith[8], R. Sobie[26], S. Söldner-Rembold[16,d], F. Spano[9], A. Stahl[3,x], K. Stephens[16], D. Strom[19], R. Ströhmer[31], S. Tarem[21], M. Tasevsky[8,z], R. Teuscher[9], M.A. Thomson[5], E. Torrence[19], D. Toya[23], P. Tran[4], I. Trigger[8], Z. Trócsányi[30,e], E. Tsur[22], M.F. Turner-Watson[1], I. Ueda[23], B. Ujvári[30,e], C.F. Vollmer[31], P. Vannerem[10], R. Vértesi[30,e], M. Verzocchi[17], H. Voss[8,q], J. Vossebeld[8,h], D. Waller[6], C.P. Ward[5], D.R. Ward[5], P.M. Watkins[1], A.T. Watson[1], N.K. Watson[1], P.S. Wells[8], T. Wengler[8], N. Wermes[3], D. Wetterling[11] G.W. Wilson[16,k], J.A. Wilson[1], G. Wolf[24], T.R. Wyatt[16], S. Yamashita[23], D. Zer-Zion[4], L. Zivkovic[24]

[1]School of Physics and Astronomy, University of Birmingham, Birmingham B15 2TT, UK
[2]Dipartimento di Fisica dell' Università di Bologna and INFN, I-40126 Bologna, Italy

[3]Physikalisches Institut, Universität Bonn, D-53115 Bonn, Germany
[4]Department of Physics, University of California, Riverside CA 92521, USA
[5]Cavendish Laboratory, Cambridge CB3 0HE, UK
[6]Ottawa-Carleton Institute for Physics, Department of Physics, Carleton University, Ottawa, Ontario K1S 5B6, Canada
[8]CERN, European Organisation for Nuclear Research, CH-1211 Geneva 23, Switzerland
[9]Enrico Fermi Institute and Department of Physics, University of Chicago, Chicago IL 60637, USA
[10]Fakultät für Physik, Albert-Ludwigs-Universität Freiburg, D-79104 Freiburg, Germany
[11]Physikalisches Institut, Universität Heidelberg, D-69120 Heidelberg, Germany
[12]Indiana University, Department of Physics, Bloomington IN 47405, USA
[13]Queen Mary and Westfield College, University of London, London E1 4NS, UK
[14]Technische Hochschule Aachen, III Physikalisches Institut, Sommerfeldstrasse 26-28, D-52056 Aachen, Germany
[15]University College London, London WC1E 6BT, UK
[16]Department of Physics, Schuster Laboratory, The University, Manchester M13 9PL, UK
[17]Department of Physics, University of Maryland, College Park, MD 20742, USA
[18]Laboratoire de Physique Nucléaire, Université de Montréal, Montréal, Québec H3C 3J7, Canada
[19]University of Oregon, Department of Physics, Eugene OR 97403, USA
[20]CCLRC Rutherford Appleton Laboratory, Chilton, Didcot, Oxfordshire OX11 0QX, UK
[21]Department of Physics, Technion-Israel Institute of Technology, Haifa 32000, Israel
[22]Department of Physics and Astronomy, Tel Aviv University, Tel Aviv 69978, Israel
[23]International Centre for Elementary Particle Physics and Department of Physics, University of Tokyo, Tokyo 113-0033, and Kobe University, Kobe 657-8501, Japan
[24]Particle Physics Department, Weizmann Institute of Science, Rehovot 76100, Israel
[25]Universität Hamburg/DESY, Institut für Experimentalphysik, Notkestrasse 85, D-22607 Hamburg, Germany
[26]University of Victoria, Department of Physics, P O Box 3055, Victoria BC V8W 3P6, Canada
[27]University of British Columbia, Department of Physics, Vancouver BC V6T 1Z1, Canada
[28]University of Alberta, Department of Physics, Edmonton AB T6G 2J1, Canada
[29]Research Institute for Particle and Nuclear Physics, H-1525 Budapest, P O Box 49, Hungary
[30]Institute of Nuclear Research, H-4001 Debrecen, P O Box 51, Hungary
[31]Ludwig-Maximilians-Universität München, Sektion Physik, Am Coulombwall 1, D-85748 Garching, Germany
[32]Max-Planck-Institute für Physik, Föhringer Ring 6, D-80805 München, Germany
[33]Yale University, Department of Physics, New Haven, CT 06520, USA

[a] and at TRIUMF, Vancouver, Canada V6T 2A3
[c] and Institute of Nuclear Research, Debrecen, Hungary
[d] and Heisenberg Fellow
[e] and Department of Experimental Physics, University of Debrecen, Hungary
[f] and MPI München
[g] and Research Institute for Particle and Nuclear Physics, Budapest, Hungary
[h] now at University of Liverpool, Dept of Physics, Liverpool L69 3BX, U.K.
[i] and CERN, EP Div, 1211 Geneva 23
[j] and Manchester University

[k] now at University of Kansas, Dept of Physics and Astronomy, Lawrence, KS 66045, U.S.A.
[l] now at University of Toronto, Dept of Physics, Toronto, Canada
[m] current address Bergische Universität, Wuppertal, Germany
[n] now at University of Mining and Metallurgy, Cracow, Poland
[o] now at University of California, San Diego, U.S.A.
[p] now at Physics Dept Southern Methodist University, Dallas, TX 75275, U.S.A.
[q] now at IPHE Université de Lausanne, CH-1015 Lausanne, Switzerland
[r] now at IEKP Universität Karlsruhe, Germany
[s] now at Universitaire Instelling Antwerpen, Physics Department, B-2610 Antwerpen, Belgium
[t] now at RWTH Aachen, Germany
[u] and High Energy Accelerator Research Organisation (KEK), Tsukuba, Ibaraki, Japan
[v] now at University of Pennsylvania, Philadelphia, Pennsylvania, USA
[w] now at TRIUMF, Vancouver, Canada
[x] now at DESY Zeuthen
[y] now at CERN
[z] now with University of Antwerp
[a1] now at DESY
[*] Deceased

1 Introduction

Gluon jets were first observed in 1979 [1], at the PETRA e^+e^- collider at DESY. Certain features of the jets were quickly measured, such as their production angular distributions, leading, for example, to a determination of the gluon spin [2]. In contrast, it has proved difficult to obtain meaningful information about internal characteristics of gluon jets. The difficulty arises because gluon jets are usually produced in conjunction with other jets or the beam remnants at accelerators, making their identification ambiguous. Gluon jets in e^+e^- annihilations are usually studied using three-jet $q\overline{q}g$ events, for example, where q denotes a quark jet, $\overline{q}$ an antiquark jet, and g a gluon jet. At hadron colliders, gluon jets are studied using events with two energetic gluon jets produced in conjunction with the beam remnants and less energetic jets. In either case, the gluon jets are identified using jet finding algorithms such as the $k_\perp$ [3] or cone [4] jet finder, which assign particles in an event to the jets. The jet finding algorithms employ resolution criteria. Different jet algorithms or choices of the resolution scales yield different assignments of particles to the jets. This produces the ambiguities mentioned above. Many studies employ fixed values for the resolution scales, leading to truncation of higher order radiation from the jets and thus to further ambiguity. Because of these intrinsic ambiguities, jets defined in this manner are called "biased."

Theoretical descriptions of gluon jets are usually based on a different approach. The theoretical approach assumes the production of a pair of gluons in an overall color singlet, i.e. gg events from a point source. There are neither beam remnants nor other jets. The gg system is divided into hemispheres in a frame in which the two gluons are back-to-back (they move in opposite directions), using the plane perpendicular to the direction of the separating gluons. The particles in a hemisphere define a jet. Since all particles in the event arise from one of the two original gluons, there is no ambiguity about which particles to assign to the gluon jets.[1] Furthermore, there are no jet resolution criteria and thus no truncation of higher order radiation, i.e. all events in the sample are used. The properties of the jets depend on a single scale: the jet energy. Jets defined in this manner are called "unbiased," in contrast to biased jets, whose properties depend on the jet resolution scales as well. Many theoretical results have been presented for unbiased gluon jets, based on Quantum Chromodynamics (QCD), the gauge theory of strong interactions. Because most experimental studies are performed using biased jets, tests of the theory have often been indirect.

So far, only three methods have been used to measure gluon jet properties in a manner consistent with the theoretical prescription outlined in the previous paragraph, avoiding the ambiguities associated with biased jets. First, radiative Υ decays, $\Upsilon \to \gamma gg \to \gamma + \textit{hadrons}$, have been studied [5, 6]. The gg system in these events corresponds to the event class of the theoretical approach, described above. Second, rare events from hadronic $Z^0 \to q\overline{q}$ decays have been selected [7–9], in which the q and $\overline{q}$ jets are approximately colinear: the event hemisphere "$g_{\text{incl.}}$" against which the q and $\overline{q}$ recoil corresponds almost exactly to an unbiased gluon jet as shown in [10]. Third, the theoretical formalism of [11] has been applied [12] to extract properties of unbiased gluon jets indirectly, by subtracting results obtained from two-jet $q\overline{q}$

[1] Note that if the event is boosted along the gg event axis, the jet energies and multiplicities change. The relationship between an unbiased jet's energy and its mean particle multiplicity is universal, however, independent of this boost or of the invariant mass of the gg system. The same comment applies to the $q\overline{q}$ color singlet systems discussed in Sect. 2.

events from those obtained from three-jet $q\overline{q}g$ events (see [11, 12] for more details).

The first and second of the above techniques provide an explicit association of particles in an event to the gluon jets. This allows many characteristics of the jets, e.g. the distributions of particle multiplicity and energy, to be studied. The jet energies associated with these two techniques are limited, however, to $E_{\rm jet} \sim 5$ and 40 GeV, respectively. The third technique, based on comparing results from $q\overline{q}$ and $q\overline{q}g$ events, yields measurements over a range of jet energies, from about 5 to 15 GeV. This method does not associate particles in an event with the gluon jet, however, yielding only the mean particle multiplicity of the jets, $\langle n_{\rm gluon} \rangle$.

In [13], an additional method to determine properties of unbiased gluon jets is proposed: the so-called jet boost algorithm. The jet boost algorithm is described in Sect. 2. So far, no experimental results have been presented based on this technique. Like the third method mentioned above, the jet boost algorithm provides results over a range of jet energies. Like the first and second methods, it specifies which particles in an event to associate with the gluon jet. The jet boost method therefore combines features of the other approaches, offering a means to measure a variety of properties of unbiased gluon jets as a function of energy.

In this paper, we present the first experimental study to use the jet boost algorithm. The study is based on hadronic decays of the Z^0 boson. The data were collected with the OPAL detector at the LEP e^+e^- storage ring at CERN. We measure the charged particle multiplicity distribution and the particle energy spectrum (fragmentation function) of the jets for a variety of jet energies. The results are compared to QCD calculations to provide new and unique tests of that theory.

2 The jet boost algorithm

The jet boost algorithm (henceforth referred to as the "boost algorithm" or "boost method") is motivated by the color dipole model of QCD [14]. Thus consider a quark-antiquark system created from a color singlet source, e.g. $e^+e^- \to q\overline{q}$ events. Because the q and $\overline{q}$ carry opposite color charges, they form a dipole. Unbiased quark jets are defined by dividing the event in half in a frame in which the q and $\overline{q}$ move back-to-back, using the plane perpendicular to the direction of the separating q and $\overline{q}$ (see Fig. 1a). This is analogous to the definition of unbiased gluon jets presented in the introduction. Note that the back-to-back frame is not necessarily the center-of-momentum (c.m.) frame of the dipole. The energy scales of the jets, $E^*_{\rm q}$ and $E^*_{\overline{\rm q}}$, are given by the hemisphere energies in the back-to-back frame. If a Lorentz boost is performed along the hemisphere boundary assuming the q and $\overline{q}$ are massless, the dipole appears as shown in Fig. 1b. In Appendix A.1 it is shown that the Lorentz β factor relating the back-to-back and boosted frames is $\beta = \cos\alpha$, where $\alpha = \theta/2$ with θ the angle between the q and $\overline{q}$ in the boosted frame. Furthermore, it is shown that the jet energies in the boosted frame, E'_i (with $i =$ q or $\overline{q}$), are related to the jet energies in the back-to-back frame, E^*_i, by

$$E^*_i = E'_i \sin\frac{\theta}{2} \quad . \tag{1}$$

In $e^+e^- \to q\overline{q}g$ events, the color charge of the gluon can be decomposed into two parts: one equal and opposite to the color charge of the quark and the other equal and opposite to

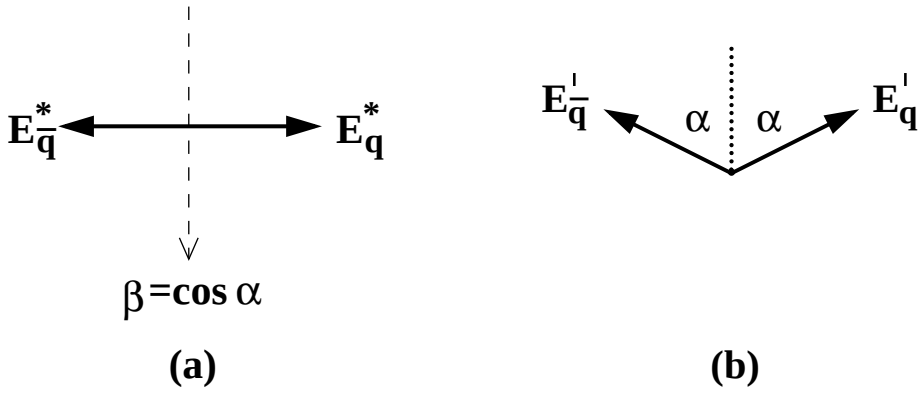

Figure 1: Schematic illustration of a $q\overline{q}$ color dipole viewed (a) in a frame in which the q and $\overline{q}$ are back-to-back, and (b) in a frame boosted in a direction bisecting the dipole. The quark and antiquark jets are labelled by their energies: E^*_q and $E^*_{\overline{q}}$ in the back-to-back frame and E'_q and $E'_{\overline{q}}$ in the boosted frame.

the charge of the antiquark. A $q\overline{q}g$ event therefore consists of two independent dipoles, one defined by the q and g and the other by the $\overline{q}$ and g. In a frame in which the angle $\theta = 2\alpha$ between the q and g is the same as the angle between the $\overline{q}$ and g, yielding a symmetric event as in Fig. 2a, each dipole can be independently boosted to a back-to-back frame along the bisector of the dipole using the boost factor $\beta = \cos\alpha$ mentioned above, again assuming the partons are massless (see Fig. 2b). The two dipoles in the back-to-back frames can then be combined to yield an event with the color structure of a gg event in a color singlet, i.e. two back-to-back gluon jet hemispheres (see Fig. 2c), since the combined quark-antiquark system has the color structure of the gluon jet as mentioned above. This corresponds to the production of unbiased gluon jets as discussed in the introduction. In the frame of the symmetric event (Fig. 2a), the unbiased gluon jet is defined by the particles in a cone of half angle α around the gluon jet axis [13]. The energy of the unbiased gluon jet, E^*_g (Fig. 2c), is related to the energy of the gluon jet in the symmetric $q\overline{q}g$ event, E'_g (Fig. 2a), by eq. (1) with $i = g$, as follows from the correspondence between Figs. 1 and 2.

Three-jet $q\overline{q}g$ events from e^+e^- annihilations are usually identified using a jet finding algorithm. Some of the most common jet finders are based on a transverse momentum cutoff, $p_{\perp,\,\mathrm{cut}}$, to resolve the jets. Examples of such algorithms are the $k_\perp$, Cambridge [15] and Luclus [16] jet finders. The value of $p_{\perp,\,\mathrm{cut}}$ (sometimes referred to as the virtuality scale [13]) specifies the maximum transverse momentum of radiated particles within a jet. As a necessary but not sufficient condition to avoid biasing the jets, $p_{\perp,\,\mathrm{cut}}$ should be adjusted separately for each event so that exactly three jets are reconstructed. In contrast, a fixed value of $p_{\perp,\,\mathrm{cut}}$ truncates higher order radiation in the jet. For gluon jets identified in this manner, any radiation ("sub-jet") emitted within the jet must necessarily have a smaller transverse momentum than the gluon jet itself, otherwise the roles of the "sub-jet" and "gluon jet" would be reversed. Thus the transverse momentum of the gluon jet, $p_{\perp,\,\mathrm{gluon}}$, defines an effective cutoff for sub-jet radiation, i.e. $p_{\perp,\,\mathrm{cut}} = p_{\perp,\,\mathrm{gluon}}$. Note that the definition of transverse momentum is ambiguous in events with hard, acolinear gluon radiation (for a discussion, see e.g. [11]). In the color dipole model,

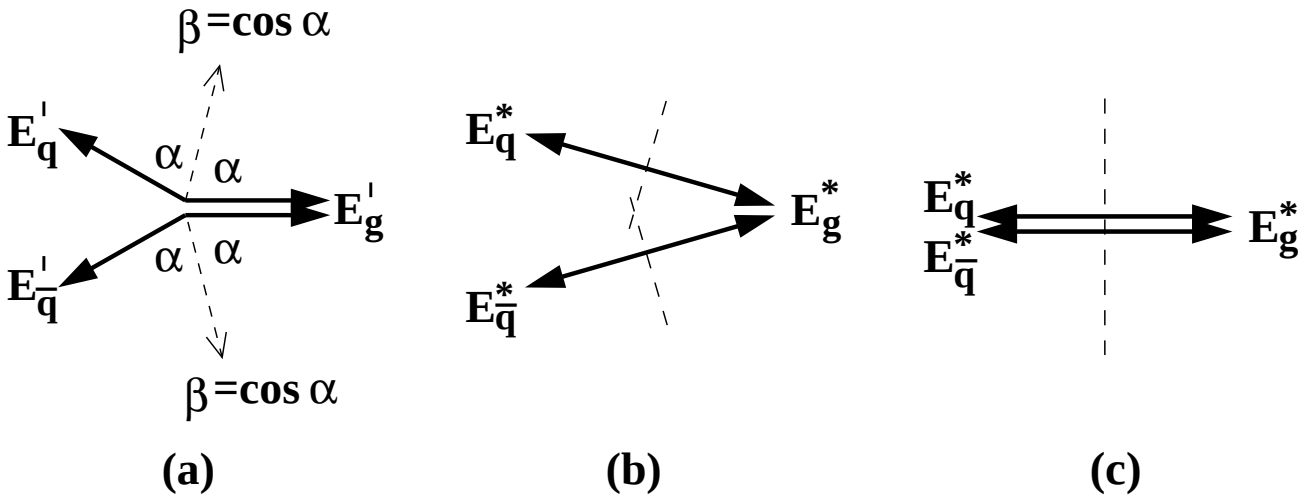

Figure 2: (a) A symmetric three-jet $q\overline{q}g$ event in which the angle $\theta = 2\alpha$ between the quark and gluon jets is the same as the angle between the antiquark and gluon jets. In the QCD dipole model, the $q\overline{q}g$ event consists of two independent color dipoles. (b) Each of the dipoles can be independently boosted to a back-to-back frame. (c) The dipoles in the back-to-back frames can be combined to yield an event with the color structure of a gluon-gluon event in a color singlet. Note that the combined quark-antiquark jet system in $e^+e^- \to q\overline{q}g$ events has the color structure of a gluon jet.

the transverse momentum of a gluon jet in a $q\overline{q}g$ event is defined by [11]

$$p_{\perp,\,\mathrm{gluon}} = \frac{1}{2}\sqrt{\frac{s_{\mathrm{qg}}s_{\overline{\mathrm{q}}\mathrm{g}}}{s}} \quad , \tag{2}$$

where s_{ij} $(i,j = \mathrm{q},\,\overline{\mathrm{q}},\,\mathrm{g})$ is the invariant mass squared of the ij pair, and $s = E^2_{\mathrm{c.m.}}$ with $E_{\mathrm{c.m.}}$ the event energy in the c.m. frame. Thus eq. (2) defines the virtuality scale of gluon jets in the $q\overline{q}g$ events. An experimental demonstration that $p_{\perp,\,\mathrm{gluon}}$ is an appropriate scale for gluon jets in $q\overline{q}g$ events is presented in [12].

For a gluon jet to be unbiased, its properties should be independent of the jet resolution scale(s). In [13] it is noted that independence from the resolution scales implies that the energy and virtuality scales are the same:

$$E^*_{\mathrm{g}} = p_{\perp,\,\mathrm{gluon}} \quad . \tag{3}$$

The boost algorithm prescription for identifying an unbiased gluon jet is then as follows [13]. Three-jet events are defined using a transverse momentum based jet algorithm. The resolution parameter of the algorithm is adjusted for every event so that exactly three jets are reconstructed. After identification of the gluon jet using standard experimental techniques (see e.g. Sect. 4), the event is boosted to the symmetric frame in which the angle between the gluon and quark jets is the same as the angle between the gluon and antiquark jets, as in Fig. 2a. The algebra of this boost is uniquely specified by the requirement of eq. (3) (see Appendix A.2). In the symmetric frame, the unbiased gluon jet is defined by all particles in a cone of half angle $\alpha = \theta/2$ around the gluon jet direction, where θ is the angle between the gluon jet and the other two jets (cf. Fig. 2a and the discussion above). The energy of the unbiased jet, E^*_{g}, is given by eqs. (2) and (3).

3 Detector and data sample

The OPAL detector is described in detail elsewhere [17, 18]. OPAL operated from 1989 to 2000. The analysis presented here is based on the tracking system and electromagnetic calorimeter. The tracking system consisted of a silicon microvertex detector, an inner vertex chamber, a large volume jet chamber, and specialized chambers at the outer radius of the jet chamber to improve the measurements in the z-direction.[2] The tracking system covered the region $|\cos\theta| < 0.98$ and was enclosed by a solenoidal magnet coil with an axial field of 0.435 T. Electromagnetic energy was measured by a lead-glass calorimeter located outside the magnet coil, which also covered $|\cos\theta| < 0.98$.

The present analysis is based on a sample of about 3.13 million hadronic annihilation events, corresponding to the OPAL sample collected within 3 GeV of the Z^0 peak (m_Z) from 1993 to 2000. This sample includes readout of both the r–ϕ and z coordinates of the silicon strip microvertex detector [18]. The procedures for identifying hadronic annihilation events are described in [19].

We employ the tracks of charged particles reconstructed in the tracking chambers and clusters of energy deposited in the electromagnetic calorimeter. Tracks are required to have at least 20 measured points (of 159 possible) in the jet chamber, or at least 50% of the number of points expected based on the track's polar angle, whichever is larger. In addition, the tracks are required to have a momentum component perpendicular to the beam axis greater than 0.05 GeV/c, to lie in the region $|\cos\theta| < 0.96$, to point to the origin to within 5 cm in the r–ϕ plane and 30 cm in the z direction, and to yield a reasonable χ^2 per degree-of-freedom for the track fit in the r–ϕ plane. Electromagnetic clusters are required to have an energy greater than 0.10 GeV if they are in the barrel section of the detector ($|\cos\theta| < 0.82$) or 0.25 GeV if they are in the endcap section ($0.82 < |\cos\theta| < 0.98$). A matching algorithm [20] is used to reduce double counting of energy in cases where charged tracks point towards electromagnetic clusters. Specifically, if a charged track points towards a cluster, the cluster's energy is re-defined by subtracting the energy that is expected to be deposited in the calorimeter by the track. If the energy of the cluster is smaller than this expected energy, the cluster is not used. In this way, the energies of the clusters are primarily associated with neutral particles.

Each accepted track and cluster is considered to be a particle. Tracks are assigned the pion mass. Clusters are assigned zero mass since they originate mostly from photons.

To eliminate residual background and events in which a significant number of particles is lost near the beam direction, the number of accepted charged tracks in an event is required to be at least five and the thrust axis of the event, calculated using the particles, is required to satisfy $|\cos(\theta_{\rm thrust})| < 0.90$, where $\theta_{\rm thrust}$ is the angle between the thrust and beam axes. The number of events which pass these cuts is about 2.77 million. The residual background to this sample from all sources is estimated to be less than 1% and is neglected.

[2] Our right handed coordinate system is defined so that z is parallel to the e^- beam axis, x points towards the center of the LEP ring, r is the coordinate normal to the beam axis, ϕ is the azimuthal angle around the beam axis with respect to x, and θ is the polar angle with respect to z.

4 Gluon jet selection

We apply the $k_\perp$ jet finder to the sample of events described in Sect. 3. The resolution scale, y_{cut}, is adjusted separately for each event so that exactly three jets are reconstructed. Both charged and neutral particles are used for the definition of the jets. The jets are assigned energies using the technique of calculated energies with massless kinematics (see for example [21]). Jet energies determined in this manner are more accurate than visible jet energies, with the latter defined by a sum over the reconstructed energies of the particles assigned to the jet. We employ massless kinematics because the boost algorithm assumes massless jets (see Sect. 2 and the Appendices). The jets are ordered such that jet 1 has the largest energy and jet 3 the smallest energy.

Due to the gluon radiation spectrum in $e^+e^- \to q\overline{q}g$ events, jet 1 is likely to be a quark (q or $\overline{q}$) jet. We therefore assume jet 1 is always a quark jet. We then use the technique of displaced secondary vertices to identify the other quark jet. Displaced secondary vertices are associated with heavy quark decay, especially that of the b quark. At LEP, b quarks are produced almost exclusively at the electroweak vertex: thus a jet containing a b hadron is almost always a quark jet. To reconstruct secondary vertices in jets, we use the method described in [22]. For jets with a secondary vertex, the signed decay length, L, is calculated with respect to the primary vertex, along with its uncertainty, σ_L. To be tagged as a quark jet, a jet is required to contain a successfully reconstructed secondary vertex with $L/\sigma_L > 3.0$. We select events for which exactly one of the lower energy jets is tagged as a quark jet. The remaining lower energy jet in these events is identified as the gluon jet.

We next examine the selected events as a function of the energy E_g^* (see eq. (3)) of the identified gluon jet. E_g^* is calculated using the jet 4-momenta in the laboratory frame and the Lorentz invariant expression eq. (2). We require E_g^* to be at least 5.0 GeV so that the jet is well defined. For $5.0 \le E_g^* < 9.5$ GeV, the estimated gluon jet purity is about 80% or larger once the final selection cuts have been applied (see below). For values of E_g^* above this, the purity is lower because the assumption that jet 1 is a quark jet becomes less accurate as the gluon jet energy increases. Therefore, for $E_g^* \ge 9.5$ GeV, we impose additional requirements on the two identified quark jets. A quark jet in an event with $9.5 \le E_g^* < 16.0$ GeV is required to contain a successfully reconstructed secondary vertex with $L/\sigma_L > 3.0$ if it is either jet 1 or 2, or $L/\sigma_L > 5.0$ if it is jet 3. These cuts account for the fact that the L/σ_L distributions of jets depend upon the jet energy. For events with $16.0 \le E_g^* < 20.0$ GeV, a quark jet is required to contain a secondary vertex with $L/\sigma_L > 5.0$ irrespective of whether it is jet 1, 2 or 3. We retain events in which the two identified quark jets (as defined in the previous paragraph) satisfy these more stringent requirements. We do not consider gluon jets with $E_g^* \ge 20.0$ GeV because of the low event statistics.

The resulting $q\overline{q}g$ sample contains many events with soft or nearly colinear jets. To eliminate these events, we impose cuts on the jet energies and angles with respect to the other jets. Besides the requirement $E_g^* \ge 5.0$ GeV for gluon jets, mentioned above, we determine the following scale for quark jets in the laboratory frame:

$$\kappa_{\rm jet} = E_{\rm jet} \, \sin\left(\frac{\theta_{\rm min.}}{2}\right) \quad , \tag{4}$$

with $\theta_{\rm min.}$ the smaller of the angles between the jet under consideration and the other two jets. The scale eq. (4) was proposed in [23] (see also [24]). Note the similarity between eqs. (1)

Bin in E_g^* (GeV)	Number of jets	$\langle E_g^* \rangle$ (GeV)	Purity (%)
5.0–5.5	4022	$5.25 \pm 0.01 \pm 0.01$	$88.8 \pm 0.4 \pm 1.4$
5.5–6.5	6652	$5.98 \pm 0.01 \pm 0.01$	$87.3 \pm 0.3 \pm 1.6$
6.5–7.5	5017	$6.98 \pm 0.01 \pm 0.01$	$84.2 \pm 0.4 \pm 2.3$
7.5–9.5	7390	$8.43 \pm 0.01 \pm 0.01$	$79.2 \pm 0.3 \pm 2.2$
9.5–13.0	1713	$10.92 \pm 0.02 \pm 0.04$	$94.5 \pm 0.3 \pm 3.6$
13.0–16.0	485	$14.24 \pm 0.04 \pm 0.05$	$86.1 \pm 0.9 \pm 4.2$
16.0–20.0	117	$17.72 \pm 0.11 \pm 0.21$	$73.9 \pm 2.5 \pm 8.9$
5.0–20.0	25 396	$7.32 \pm 0.01 \pm 0.07$	$85.1 \pm 0.2 \pm 2.6$

Table 1: Bins in the unbiased jet energy E_g^*, and the corresponding number of jets, mean energies, and estimated purities, for the gluon jets in our final event sample. The last row gives the results for the entire sample. For the $\langle E_g^* \rangle$ and purity results, the first uncertainty is statistical and the second systematic.

and (4). We require the quark jets to satisfy $\kappa_{\rm jet} \geq 8.0$ GeV. After applying all cuts, the number of selected events is 25 396.

The purity of this sample is evaluated using simulated events generated with the Herwig Monte Carlo event generator, version 6.2 [25]. Herwig is chosen because it is known to provide a better description of gluon jets in e^+e^- annihilations than the available alternatives (see e.g. [7]). The Monte Carlo events are examined at the "detector level." The detector level includes initial-state photon radiation, simulation of the OPAL detector [26], and the same analysis procedures as are applied to the data. The detector level Herwig sample in our study contains six million inclusive Z^0 events. The parameter values we use for Herwig are documented in [27]. We determine the directions of the primary quark and antiquark from the Z^0 decay after the parton shower has terminated. The reconstructed jet closest to the direction of an evolved primary quark or antiquark is considered to be a quark jet. The distinct jet closest to the evolved primary quark or antiquark not associated with this first jet is considered to be the other quark jet. The remaining jet is the gluon jet. Using this method, the overall purity of the final gluon jet sample is found to be $85.1 \pm 0.2\,(\text{stat.})\%$.

The data are binned in seven intervals of E_g^*. The bin edges are chosen so that the mean gluon jet energy for most bins corresponds to an energy at which unbiased quark jet multiplicity data are available for comparison (see Sect. 9.1.3). Table 1 summarizes the bin definition, number of gluon jets, mean jet energy $\langle E_g^* \rangle$ and estimated gluon jet purity, for each bin. The systematic uncertainties attributed to the $\langle E_g^* \rangle$ and purity results are discussed in Sect. 8.

The boost algorithm (Sect. 2) is applied to the selected $q\overline{q}g$ events. Henceforth, by "gluon jet," we refer to gluon jets treated according to this prescription.

Because we rely on b quark tagging to identify gluon jets, the events we study are enriched in heavy quark jets. This is in apparent contradiction with the assumption of the boost algorithm that the jets are massless. The Herwig Monte Carlo predicts that about 80% of the events in the final sample are b events. In Sect. 6, we show that this reliance on b events does not affect the applicability of the method (see Fig. 6 below). Also note that the properties of hard, acolinear

gluon jets do not depend on the event flavor according to QCD, as has been experimentally demonstrated in e.g. [28].

5 Experimental distributions

We study the charged particle multiplicity distributions of the identified gluon jets, $n^{\mathrm{ch.}}_{\mathrm{gluon}}$. The multiplicity distributions are presented in terms of their fractional probabilities, $P(n^{\mathrm{ch.}}_{\mathrm{gluon}})$, and are thus normalized to have unit area. We also study the fragmentation functions of the jets. The fragmentation function $1/N\,(\mathrm{d}n^{\mathrm{ch.}}_{\mathrm{gluon}}/\mathrm{d}x^*_E)$ is defined by the inclusive distribution of scaled charged particle energies $x^*_E = E^*/E^*_{\mathrm{g}}$ in the back-to-back frames of the qg and $\overline{\mathrm{q}}\mathrm{g}$ dipoles (see Fig. 2b). The fragmentation functions are normalized to the number of events N in the respective bins of E^*_{g} (see Table 1). To determine the particle energies E^*, particles assigned to the gluon jet in the symmetric frame (Fig. 2a) are boosted to the back-to-back frames of the dipoles using the boost factor $\beta = \cos\alpha$ mentioned in Sect. 2 (see also Appendix A.1). In the data, it is not possible to know the dipole with which a particle should be associated. Therefore, we tried both possibilities. We found that the same results are obtained irrespective of whether the particles are boosted to the frame of the qg or the $\overline{\mathrm{q}}\mathrm{g}$ dipole.

We also examine the mean and first two non-trivial normalized factorial moments of the $n^{\mathrm{ch.}}_{\mathrm{gluon}}$ distribution, denoted $\langle n^{\mathrm{ch.}}_{\mathrm{gluon}}\rangle$, $F_{2,\,\mathrm{gluon}}$ and $F_{3,\,\mathrm{gluon}}$, respectively. Normalized factorial moments [29] are defined by

$$F_\ell = \frac{\langle n(n-1)\cdots(n-\ell+1)\rangle}{\langle n\rangle^\ell} \quad , \tag{5}$$

with $n = n^{\mathrm{ch.}}_{\mathrm{gluon}}$ and ℓ a positive integer. Note that F_2 is directly related to the dispersion of a distribution while F_3 is related to both the skew and dispersion (see e.g. [8]). Thus normalized factorial moments provide information about the shape of a distribution, or equivalently about event-to-event fluctuations from the mean. We study normalized factorial moments because QCD predictions for the shape of multiplicity distributions are usually presented in that form (for a review, see [30]).

6 Test of the boost algorithm

Before describing our results, we present a test of the boost algorithm using events generated with the Herwig Monte Carlo event generator. With simulated events, it is possible to compare gluon jets from $\mathrm{e^+e^-}$ hadronic $\mathrm{Z^0}$ decays as used in the experiment with unbiased gluon jets from color singlet gg events as used in theoretical calculations.

The Monte Carlo events are examined at the "hadron level." The hadron level does not include initial-state radiation or detector simulation and utilizes all charged and neutral particles with lifetimes greater than 3×10^{-10} s, which are treated as stable. For the inclusive $\mathrm{Z^0}$ hadronic events, we generated a sample with 10 million events. For the gg event samples, 10 million events were generated at each energy (see below).

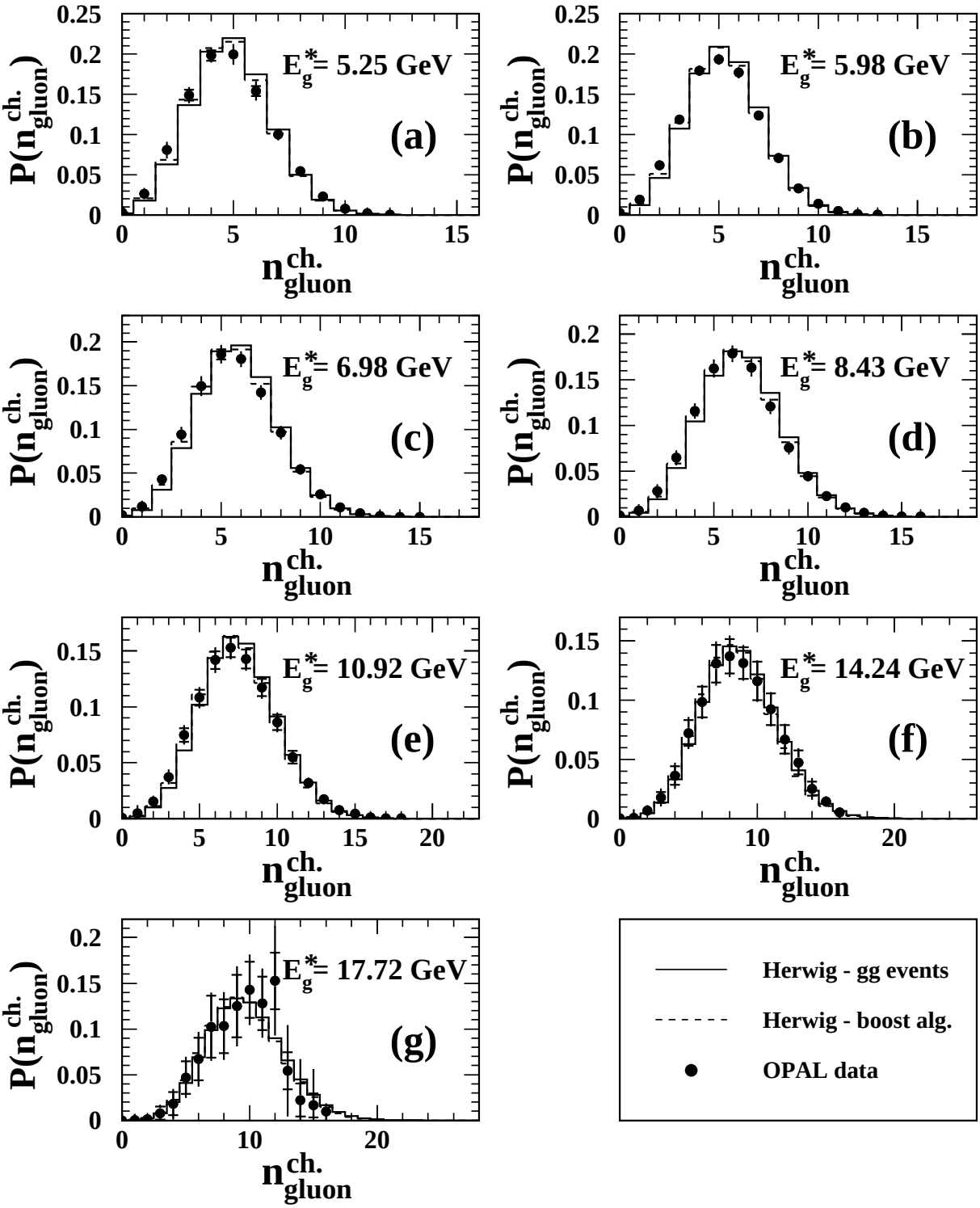

Figure 3: Charged particle multiplicity distributions of gluon jets, $n_{\rm gluon}^{\rm ch.}$, for different jet energies $E_{\rm g}^*$. The data have been corrected for detector acceptance and resolution, for event selection, and for gluon jet impurity. The total uncertainties are shown by the vertical lines, with the statistical component delimited by small horizontal lines. The data are presented in comparison to predictions of the Herwig Monte Carlo event generator at the hadron level. Two different sets of Monte Carlo results are included: one based on $\rm e^+e^-$ events treated using the boost algorithm, and one based on hemispheres of gg events.

The dashed histograms in Fig. 3 show the prediction of Herwig for the $n^{\rm ch.}_{\rm gluon}$ distributions of Z^0 events, obtained using the boost algorithm. The results are shown for the seven bins of energy $E^*_{\rm g}$ defined in Table 1. The events are selected using the procedures described in Sect. 4 for the data, except that the quark jet identification is performed using Monte Carlo information as explained in Sect. 4. The solid histograms show the corresponding results for hemispheres of gg events. The energies of the gg hemispheres are chosen to equal the mean energies of the jets obtained from the boost algorithm, for each bin. The solid points with uncertainties in Fig. 3 show our corrected data: these are discussed in Sect. 9.1.

The analogous results for the mean value $\langle n^{\rm ch.}_{\rm gluon}\rangle$ and the normalized factorial moments $F_{2,\,\rm gluon}$ and $F_{3,\,\rm gluon}$ are presented in Fig. 4. The small figures above the distributions in Fig. 4 show the fractional differences between the results of the boost and gg hemisphere methods. Note that the statistical uncertainties of these differences are much smaller than the differences themselves, as is also true for the other difference plots between the boost and gg hemisphere methods presented below.

From Fig. 3 it is seen that the results of the boost algorithm correspond well with those of the gg hemispheres. Nonetheless, a small shift towards lower $n^{\rm ch.}_{\rm gluon}$ is present in the distributions from the boost method, as is most clearly visible from the difference plot in Fig. 4a. From this plot, the shift is seen to be about 2%, independent of the energy. This difference of 2% is comparable to the experimental uncertainties (see Sect. 9.1) and no correction is made for it. From the difference plots in Figs. 4b and c, it is seen that the results for $F_{2,\,\rm gluon}$ and $F_{3,\,\rm gluon}$ from the boost method agree to better than about 1% with those of gg hemispheres, i.e. the shapes of the $n^{\rm ch.}_{\rm gluon}$ distributions found using the two methods are very similar. We conclude that the boost algorithm provides an accurate means to measure unbiased gluon jet multiplicity, at least for jet energies larger than 5 GeV.

An analogous study of the gluon jet fragmentation function is presented in Fig. 5. For $E^*_{\rm g} \gtrsim 11$ GeV (Figs. 5e–g), the results of the boost and gg hemisphere methods are seen to be in reasonable agreement, i.e. the solid and dashed curves are quite similar. For smaller energies (Figs. 5a–d), the boost algorithm predicts a significant excess of particles with large x^*_E values compared to the gg events, however. The reason the boost method more accurately describes the properties of gg events as the jet energy increases is that the assumption of massless gluon jets (Sect. 2) becomes more accurate for larger jet energies. We verified using Monte Carlo events with $E_{\rm c.m.} > m_{\rm Z}$ that the agreement between the two methods is even better for $E^*_{\rm g}$ values above those in our study.

The difference plots in the top portions of Figs. 5a–g show the fractional differences between the results of the boost and gg hemisphere methods. The difference plots for Figs. 5a–f are presented on two scales, one for $0.0 \le x^*_E \le 0.50$ and the other for $0.50 \le x^*_E \le 1.00$, to improve their visibility. For $E^*_{\rm g} \le 10.92$ GeV (Figs. 5a-e), the results of the boost algorithm are seen to deviate from those of the gg hemispheres by up to about 20% or more, even for $x^*_E \lesssim 0.50$ where the experimental uncertainties are relatively small (see Sect. 9.2 for a discussion of the data). For $E^*_{\rm g} = 14.24$ and 17.72 GeV (Figs. 5f and g), the deviations for $x^*_E \lesssim 0.50$ are at most about 10% and in most x^*_E bins much less. In our study of the gluon jet fragmentation function (Sect. 9.2), we therefore restrict our attention to the jet samples with $E^*_{\rm g} = 14.24$ and 17.72 GeV.

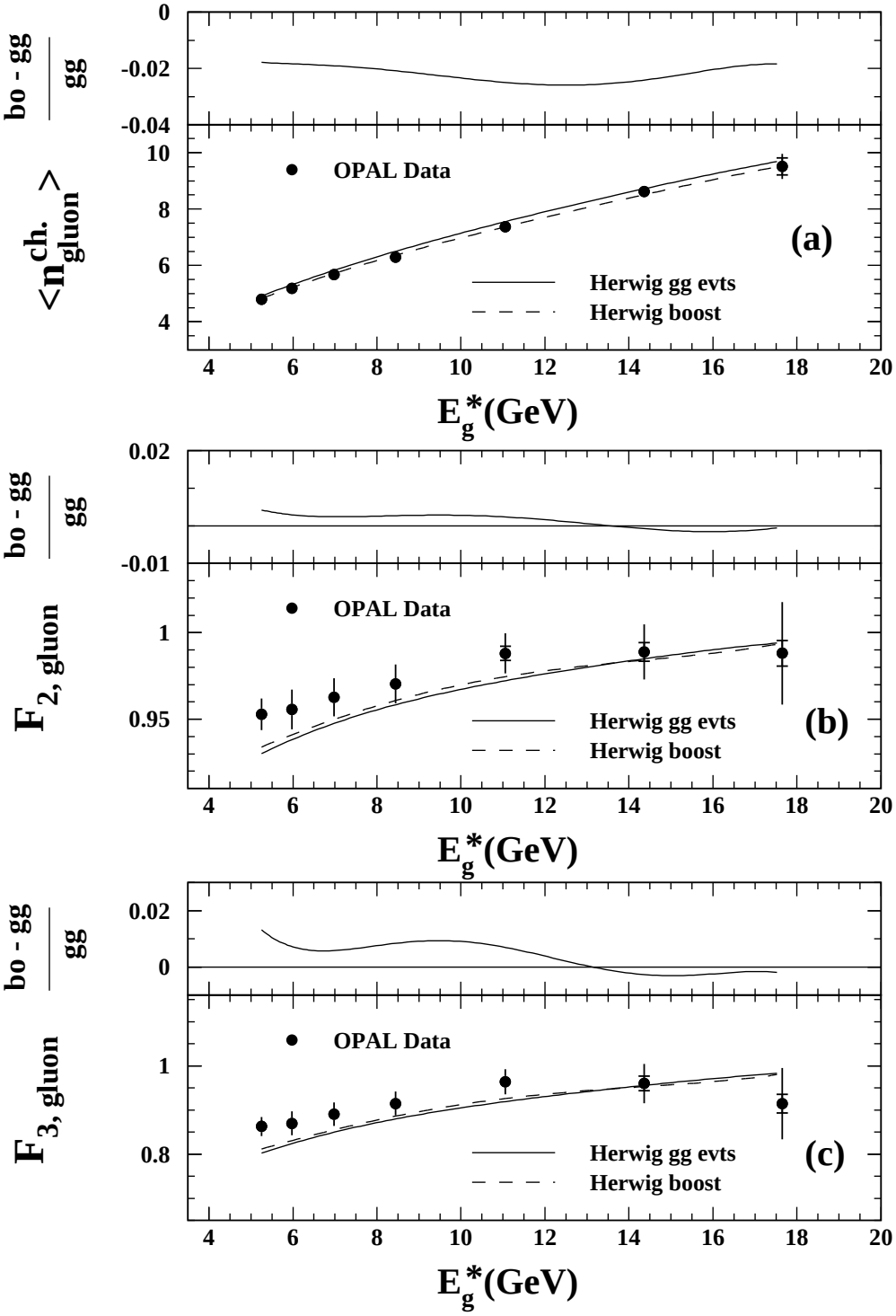

Figure 4: (a) The mean charged particle multiplicity value of gluon jets, $\langle n_{\rm gluon}^{\rm ch.} \rangle$, as a function of the gluon jet energy $E_{\rm g}^*$. (b,c) The corresponding results for the two lowest non-trivial normalized factorial moments, $F_{2,\,\rm gluon}$ and $F_{3,\,\rm gluon}$. The data have been corrected for detector acceptance and resolution, for event selection, and for gluon jet impurity. The total uncertainties are shown by the vertical lines, with the statistical component delimited by small horizontal lines. The data are presented in comparison to predictions of the Herwig Monte Carlo event generator at the hadron level. The small figures above each distribution show the fractional differences between the results of Herwig found using the boost ("bo") and gg event hemisphere ("gg") methods.

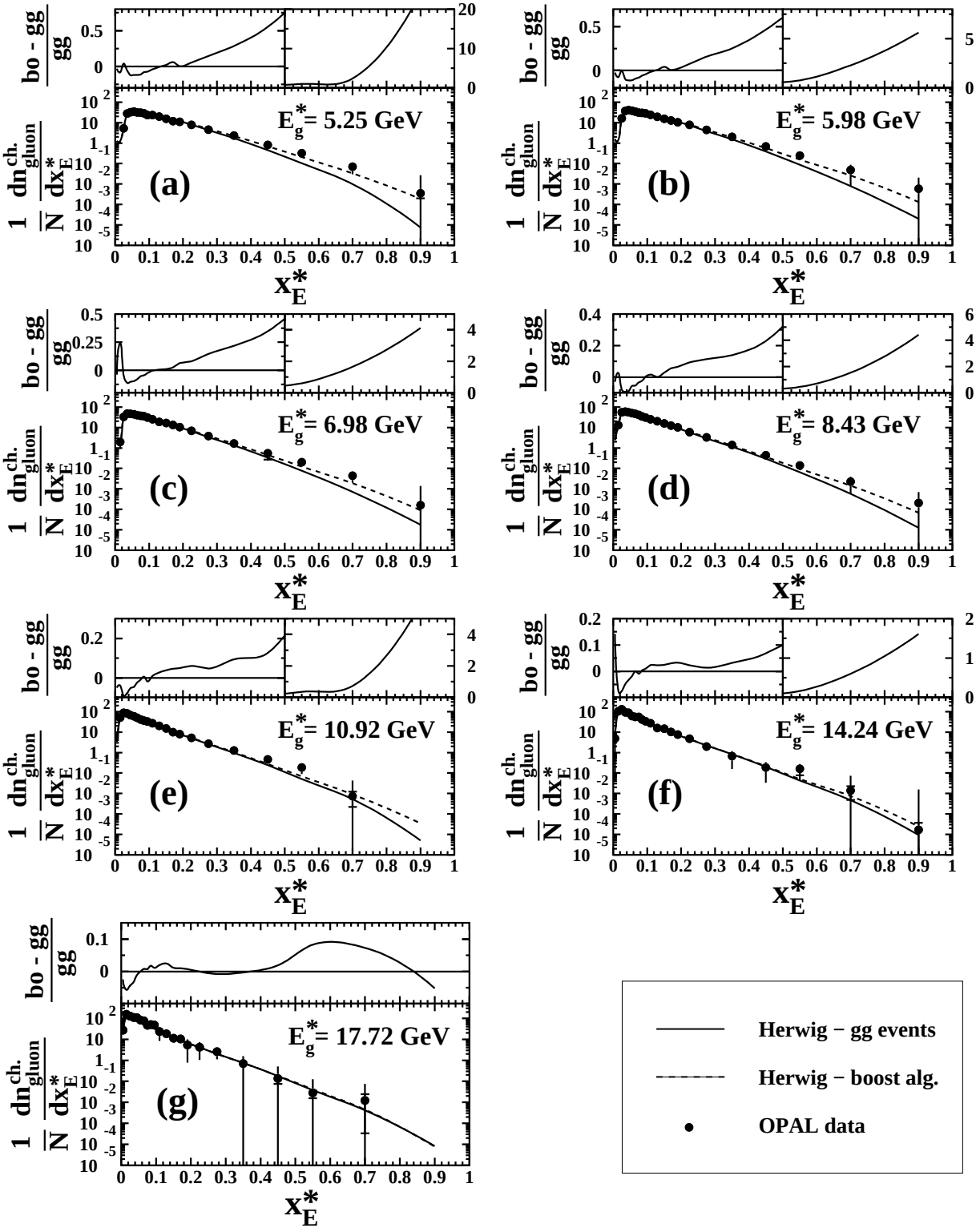

Figure 5: Charged particle fragmentation functions of gluon jets, $1/N\,(\mathrm{d}n^{\mathrm{ch.}}_{\mathrm{gluon}}/\mathrm{d}x^*_E)$, for different jet energy values E^*_{g}. The data have been corrected for detector acceptance and resolution, for event selection, and for gluon jet impurity. The total uncertainties are shown by the vertical lines, with the statistical component delimited by small horizontal lines. The data are presented in comparison to predictions of the Herwig Monte Carlo event generator at the hadron level. The small figures above each distribution show the fractional differences between the results of Herwig found using the boost ("bo") and gg event hemisphere ("gg") methods.

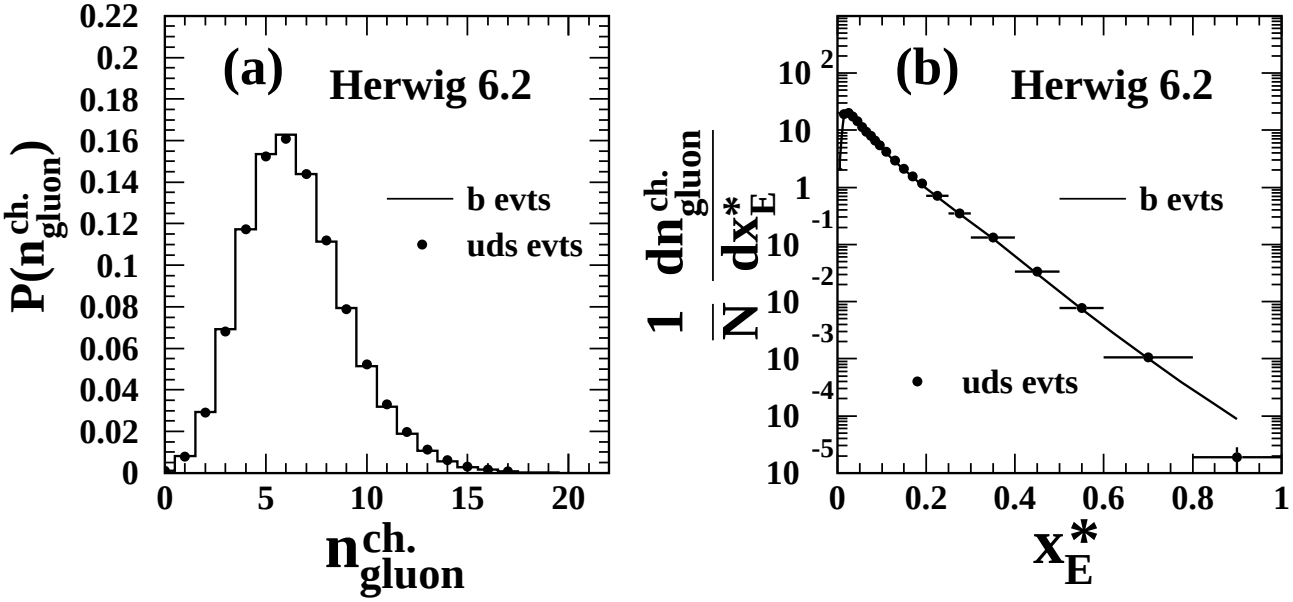

Figure 6: Hadron level results from the Herwig Monte Carlo for the (a) $n^{\mathrm{ch.}}_{\mathrm{gluon}}$ and (b) $1/N\,(\mathrm{d}n^{\mathrm{ch.}}_{\mathrm{gluon}}/\mathrm{d}x^*_E)$ distributions, for uds and b flavor events. The results in (a) are given for jet energies $5 \leq E^*_{\mathrm{g}} \leq 20$ GeV, corresponding to the range for which we find the boost method to be applicable for the $n^{\mathrm{ch.}}_{\mathrm{gluon}}$ distribution. Analogously, the results in (b) are given for $13 \leq E^*_{\mathrm{g}} \leq 20$ GeV, corresponding to the more limited range for which we find the boost method to be applicable for the $1/N\,(\mathrm{d}n^{\mathrm{ch.}}_{\mathrm{gluon}}/\mathrm{d}x^*_E)$ distribution.

Fig. 6 shows the results we obtain from applying the boost algorithm to uds and b flavor events from Herwig. For simplicity, the results for the $n^{\mathrm{ch.}}_{\mathrm{gluon}}$ distribution (Fig. 6a) include all jet energies, $5 \leq E^*_{\mathrm{g}} \leq 20$ GeV. The results for the $1/N\,(\mathrm{d}n^{\mathrm{ch.}}_{\mathrm{gluon}}/\mathrm{d}x^*_E)$ distribution (Fig. 6b) are restricted to the two highest energy bins ($13 \leq E^*_{\mathrm{g}} \leq 20$ GeV) for the reason stated in the previous paragraph. With the exception of the highest bin in Fig. 6b ($x^*_E \geq 0.80$), it is seen that the uds and b events yield essentially identical results for the gluon jet properties. This establishes that our reliance on b events to identify gluon jets (Sect. 4) does not introduce a significant bias, i.e. the theoretical assumption of massless jets is not an important consideration for the quark jets. We also tested the massless parton assumption of the boost algorithm by repeating the comparisons of the gg and boost results shown in Figs. 3–5 after scaling the charged particle 3-momenta so that the magnitude of a particle's 3-momentum equaled its energy, and found that our conclusions were unchanged.

It is interesting to establish the degree to which gluon jet properties determined using the boost method are independent of the jet algorithm chosen for the initial definition of the jets. Fig. 7a shows the Herwig prediction for the $n^{\mathrm{ch.}}_{\mathrm{gluon}}$ distribution, for jets defined using the Luclus, Cambridge, cone and Jade [31] jet finders, in addition to the $k_\perp$ jet finder used for our standard analysis. Note that the Jade algorithm uses the invariant mass between jets as a resolution criterion. The cone jet finder uses the total particle energy within a cone. These two jet finders – unlike the other three – are therefore not based on the transverse momentum $p_{\perp,\,\mathrm{cut}}$ between jets and so do not correspond to the framework of the dipole model or boost algorithm (see Sect. 2). The five jet algorithms are seen to yield essentially identical results, demonstrating the

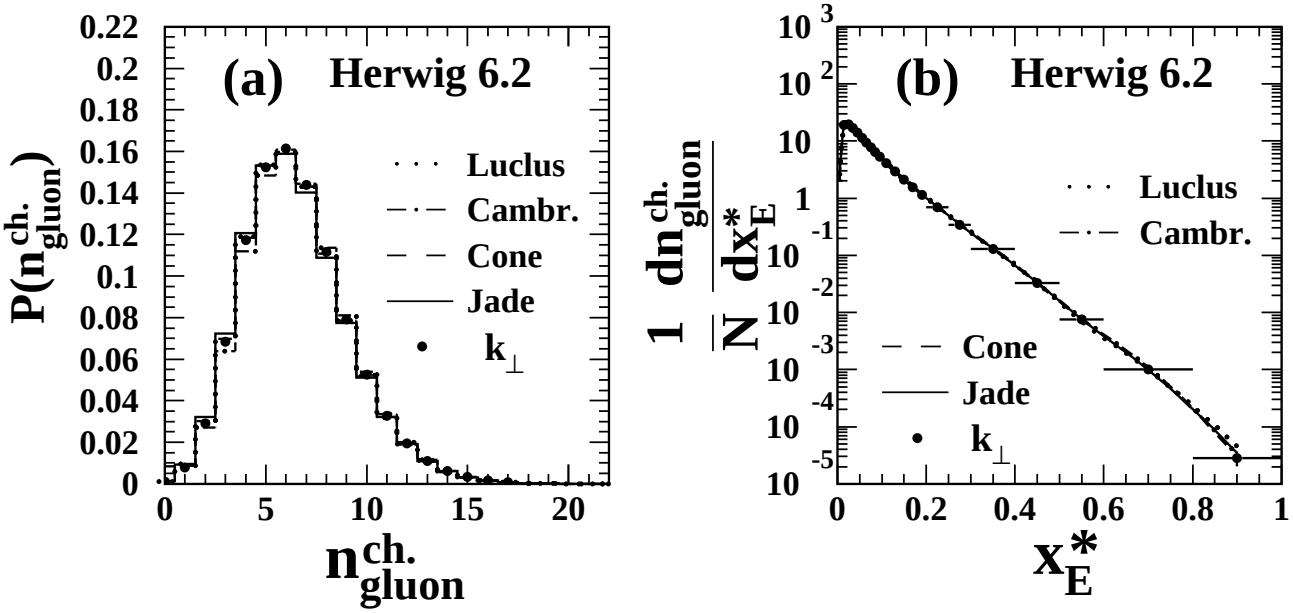

Figure 7: Hadron level results from the Herwig Monte Carlo for the (a) $n^{\mathrm{ch.}}_{\mathrm{gluon}}$ and (b) $1/N\,(\mathrm{d}n^{\mathrm{ch.}}_{\mathrm{gluon}}/\mathrm{d}x^*_E)$ distributions, for different choices of the jet finding algorithm used for the initial definition of gluon jets. The results in (a) are given for jet energies $5 \leq E^*_{\mathrm{g}} \leq 20$ GeV, corresponding to the range for which we find the boost method to be applicable for the $n^{\mathrm{ch.}}_{\mathrm{gluon}}$ distribution. Analogously, the results in (b) are given for $13 \leq E^*_{\mathrm{g}} \leq 20$ GeV, corresponding to the more limited range for which we find the boost method to be applicable for the $1/N\,(\mathrm{d}n^{\mathrm{ch.}}_{\mathrm{gluon}}/\mathrm{d}x^*_E)$ distribution.

independence of the boost method from the jet finder choice. The fact that the cone and Jade jet finders yield essentially the same results as the three $p_{\perp,\,\mathrm{cut}}$ based algorithms demonstrates the robustness of the boost algorithm in this respect. The corresponding results for the gluon jet fragmentation function are shown in Fig. 7b. Again, all five jet algorithms are seen to yield essentially identical results.

7 Correction procedure

We correct the data to the hadron level (Sect. 6) and for gluon jet impurity. This allows our data to be compared more directly to the results of other studies and to theoretical calculations (Sect. 9).

The multiplicity distributions are corrected in two steps. In the first step, the data are corrected for particle acceptance, resolution, and secondary electromagnetic and hadronic interactions using an unfolding matrix. The matrix is constructed using detector level Monte Carlo events (Sect. 4) subjected to the same analysis procedures as the data. The matrix relates the value of $n^{\mathrm{ch.}}_{\mathrm{gluon}}$ at the detector level to the corresponding value before the same event is processed by the detector simulation. In the second step, the data are corrected for event acceptance and selection, initial-state radiation and gluon jet impurity using bin-by-bin factors.

The factors are constructed by taking the ratio of hadron to detector level Monte Carlo predictions. The method of bin-by-bin corrections is described in [32]. The matrices and bin-by-bin factors are determined using Herwig. The matrices indicate that about 80% of the events exhibit a migration of one $n^{\mathrm{ch.}}_{\mathrm{gluon}}$ bin or less between the detector and hadron levels. About 50% of the events have the same value of $n^{\mathrm{ch.}}_{\mathrm{gluon}}$ at the two levels. The overall size of the corrections, including the bin-by-bin factors, varies from about 10 to 30%.

The fragmentation functions are corrected using the bin-by-bin method, also based on Herwig. A matrix procedure is not used for the fragmentation functions because they include more than one entry per event. The typical size of the corrections is 15%.

8 Systematic uncertainties

To evaluate systematic uncertainties for the corrected data, we repeated the analysis with the changes given in the list below. The differences between the standard results and those found using each of these conditions were used to define symmetric systematic uncertainties. The systematic uncertainties were added in quadrature to define the total systematic uncertainties. The systematic uncertainty evaluated for each bin was averaged with the results from its two neighbors to reduce the effect of bin-to-bin fluctuations. The single neighbor was used for bins at the ends of the distributions.

The applied changes are:

1. The Ariadne Monte Carlo [33], version 4.11, and the Jetset Monte Carlo [34], version 7.4, were used to correct the data, rather than Herwig. Samples of six million Ariadne and Jetset events at the detector level (Sect. 4) were used for this purpose. The parameter values used for these two models are given in [27] and [28], respectively.

2. Charged tracks alone were used for the data and Monte Carlo samples with detector simulation, rather than charged tracks plus electromagnetic clusters (note: in the standard analysis, electromagnetic clusters are used in the definition of the jets, see Sect. 4).

3. The particle selection was further varied, first by restricting charged tracks and electromagnetic clusters to the central region of the detector, $|\cos\theta| < 0.70$, rather than $|\cos\theta| < 0.96$ for the charged tracks and $|\cos\theta| < 0.98$ for the clusters, and second by increasing the minimum transverse momentum of charged tracks with respect to the beam axis from 0.05 GeV/c to 0.15 GeV/c.

4. The quark jet tagging requirements were changed by requiring the decay length of the lower energy quark jet to satisfy $L/\sigma_L > 2.0$ for $5.0 \leq E^*_{\mathrm{g}} < 9.5$ GeV, rather than $L/\sigma_L > 3.0$, and at the same time by requiring the decay lengths of jets 1 and 2 to satisfy $L/\sigma_L > 2.0$ for $9.5 \leq E^*_{\mathrm{g}} < 16.0$ GeV, again rather than $L/\sigma_L > 3.0$. This resulted in 35 607 events with an estimated purity of $80.5 \pm 0.1\,(\mathrm{stat.})\%$. As an additional check on the quark jet selection we increased the minimum κ_{jet} value of quark jets (see eq. (4)) from 8 to 10 GeV, with the L/σ_L requirements at their standard values. This resulted in 23 128 events with an estimated purity of $85.7 \pm 0.2\,(\mathrm{stat.})\%$.

For the first item, the largest of the described differences with respect to the standard result was assigned as the systematic uncertainty, and similarly for the third and fourth items.

The largest contribution to the systematic uncertainties generally arose from using Ariadne or Jetset to correct the data. The second largest contribution generally arose from using charged particles alone or from restricting particles to $|\cos\theta| < 0.70$.

Systematic uncertainties were also evaluated for the gluon jet purities listed in Table 1. These uncertainties were derived by repeating the analysis using each of the systematic variations given in the above list, except for item 4 since this check is specifically designed to alter the purities. The results are given in Table 1. Similarly, the systematic uncertainties listed in Table 1 for the mean gluon jet energies $\langle E_{\mathrm{g}}^{*} \rangle$ were derived using the systematic variations in the above list, except for item 1 since data at the detector level do not depend on the Monte Carlo.

9 Results

9.1 Multiplicity distributions

The corrected multiplicity distributions are shown by the solid points with uncertainties in Fig. 3. The vertical lines show the total uncertainties, with statistical and systematic terms added in quadrature. Statistical uncertainties were evaluated for the corrected data using 50 independent samples of Monte Carlo events at the hadron level, each with about the same event statistics as the data (this comment applies to all the corrected measurements presented in this paper). The statistical components of the uncertainties are delimited by small horizontal lines (for some points the statistical uncertainties are too small to be visible). These data are listed in Tables 2–4. The corresponding results for $\langle n_{\mathrm{gluon}}^{\mathrm{ch.}} \rangle$, $F_{2,\,\mathrm{gluon}}$ and $F_{3,\,\mathrm{gluon}}$ are presented in Fig. 4 and Table 5.

In Fig. 8 we again present the corrected results for $\langle n_{\mathrm{gluon}}^{\mathrm{ch.}} \rangle$, $F_{2,\,\mathrm{gluon}}$ and $F_{3,\,\mathrm{gluon}}$, this time including our direct measurements at $E_{\mathrm{g}}^{*} = 40.1$ GeV [8, 9] based on $\mathrm{e^+e^-} \to \mathrm{q\overline{q}g_{incl.}}$ events. Fig. 8a also includes a direct measurement of $\langle n_{\mathrm{gluon}}^{\mathrm{ch.}} \rangle$ from the CLEO Collaboration at $E_{\mathrm{g}}^{*} = 5.2$ GeV [5], based on radiative $\Upsilon(3S)$ decays. The open points in Fig. 8a show our earlier results [12] based on subtracting multiplicities in $\mathrm{q\overline{q}}$ and $\mathrm{q\overline{q}g}$ events [11]. The results from the present study are seen to be consistent with these latter data, and are considerably more precise. Our results are also consistent with the CLEO measurement.

From Fig. 4a (or Fig. 8a) it is seen that the energy evolution of $\langle n_{\mathrm{gluon}}^{\mathrm{ch.}} \rangle$ is well described by Herwig. The Herwig predictions for the higher moments $F_{2,\,\mathrm{gluon}}$ and $F_{3,\,\mathrm{gluon}}$ are also in reasonable agreement with the data, as seen from Figs. 4b and c (or Figs. 8b and c), although the Monte Carlo curves lie somewhat below the measurements for jet energies smaller than about 12 GeV.

In the following, we present fits of QCD expressions to the $\langle n_{\mathrm{gluon}}^{\mathrm{ch.}} \rangle$, $F_{2,\,\mathrm{gluon}}$ and $F_{3,\,\mathrm{gluon}}$ data. The theoretical expressions are at the "parton level." The corresponding distributions are denoted $\langle n_{\mathrm{gluon}}^{\mathrm{parton}} \rangle$, $F_{2,\,\mathrm{gluon}}^{\mathrm{parton}}$ and $F_{3,\,\mathrm{gluon}}^{\mathrm{parton}}$. The parton level is based on quarks and gluons present

$n_{\rm gluon}^{\rm ch.}$	$P(n_{\rm gluon}^{\rm ch.})$, $E_{\rm g}^{*}=5.25$ GeV	$P(n_{\rm gluon}^{\rm ch.})$, $E_{\rm g}^{*}=5.98$ GeV	$P(n_{\rm gluon}^{\rm ch.})$, $E_{\rm g}^{*}=6.98$ GeV
0	$0.0036 \pm 0.0009 \pm 0.0036$	$0.0025 \pm 0.0005 \pm 0.0025$	$0.0019 \pm 0.0004 \pm 0.0019$
1	$0.0266 \pm 0.0021 \pm 0.0068$	$0.0190 \pm 0.0014 \pm 0.0040$	$0.0117 \pm 0.0011 \pm 0.0069$
2	$0.0808 \pm 0.0046 \pm 0.0093$	$0.0618 \pm 0.0026 \pm 0.0048$	$0.0427 \pm 0.0022 \pm 0.0057$
3	$0.1490 \pm 0.0067 \pm 0.0078$	$0.1186 \pm 0.0046 \pm 0.0044$	$0.0943 \pm 0.0046 \pm 0.0073$
4	$0.1982 \pm 0.0063 \pm 0.0058$	$0.1794 \pm 0.0057 \pm 0.0029$	$0.1494 \pm 0.0052 \pm 0.0099$
5	$0.199 \pm 0.006 \pm 0.012$	$0.1935 \pm 0.0044 \pm 0.0050$	$0.1857 \pm 0.0058 \pm 0.0088$
6	$0.154 \pm 0.006 \pm 0.010$	$0.1769 \pm 0.0040 \pm 0.0061$	$0.1803 \pm 0.0050 \pm 0.0078$
7	$0.1000 \pm 0.0046 \pm 0.0059$	$0.1236 \pm 0.0043 \pm 0.0042$	$0.1422 \pm 0.0048 \pm 0.0069$
8	$0.0545 \pm 0.0029 \pm 0.0049$	$0.0710 \pm 0.0029 \pm 0.0024$	$0.0961 \pm 0.0044 \pm 0.0064$
9	$0.0230 \pm 0.0021 \pm 0.0012$	$0.0330 \pm 0.0020 \pm 0.0019$	$0.0543 \pm 0.0029 \pm 0.0053$
10	$0.0079 \pm 0.0012 \pm 0.0012$	$0.0139 \pm 0.0011 \pm 0.0018$	$0.0256 \pm 0.0020 \pm 0.0035$
11	$0.00232 \pm 0.00046 \pm 0.00071$	$0.0050 \pm 0.0007 \pm 0.0014$	$0.0106 \pm 0.0011 \pm 0.0020$
12	$0.00041 \pm 0.00028 \pm 0.00041$	$0.00129 \pm 0.00038 \pm 0.00077$	$0.0039 \pm 0.0007 \pm 0.0010$
13	—	$0.00034 \pm 0.00016 \pm 0.00031$	$0.00094 \pm 0.00043 \pm 0.00055$
14	—	—	$0.00017 \pm 0.00017 \pm 0.00017$
15	—	—	$0.00017 \pm 0.00006 \pm 0.00017$

Table 2: The charged particle multiplicity distribution of gluon jets, $n_{\rm gluon}^{\rm ch.}$, for $E_{\rm g}^{*}=5.25$, 5.98 and 6.98 GeV. The data have been corrected for detector acceptance and resolution, for event selection, and for gluon jet impurity. The first uncertainty is statistical and the second systematic.

$n_{\rm gluon}^{\rm ch.}$	$P(n_{\rm gluon}^{\rm ch.})$, $E_{\rm g}^{*}=8.43$ GeV	$P(n_{\rm gluon}^{\rm ch.})$, $E_{\rm g}^{*}=10.92$ GeV
0	$0.0012 \pm 0.0003 \pm 0.0012$	$0.0008 \pm 0.0004 \pm 0.0008$
1	$0.0069 \pm 0.0010 \pm 0.0066$	$0.0047 \pm 0.0012 \pm 0.0047$
2	$0.0280 \pm 0.0019 \pm 0.0075$	$0.0152 \pm 0.0028 \pm 0.0047$
3	$0.0646 \pm 0.0029 \pm 0.0078$	$0.0373 \pm 0.0043 \pm 0.0052$
4	$0.1157 \pm 0.0035 \pm 0.0075$	$0.0749 \pm 0.0060 \pm 0.0062$
5	$0.1621 \pm 0.0052 \pm 0.0085$	$0.1083 \pm 0.0071 \pm 0.0063$
6	$0.1783 \pm 0.0043 \pm 0.0080$	$0.1419 \pm 0.0080 \pm 0.0082$
7	$0.1632 \pm 0.0045 \pm 0.0086$	$0.1530 \pm 0.0087 \pm 0.0061$
8	$0.1207 \pm 0.0039 \pm 0.0073$	$0.1428 \pm 0.0085 \pm 0.0063$
9	$0.0756 \pm 0.0031 \pm 0.0064$	$0.1173 \pm 0.0075 \pm 0.0066$
10	$0.0443 \pm 0.0021 \pm 0.0053$	$0.0862 \pm 0.0070 \pm 0.0053$
11	$0.0226 \pm 0.0010 \pm 0.0031$	$0.0550 \pm 0.0055 \pm 0.0033$
12	$0.0103 \pm 0.0008 \pm 0.0020$	$0.0320 \pm 0.0034 \pm 0.0032$
13	$0.0044 \pm 0.0006 \pm 0.0012$	$0.0172 \pm 0.0031 \pm 0.0030$
14	$0.00141 \pm 0.00043 \pm 0.00071$	$0.0074 \pm 0.0019 \pm 0.0016$
15	$0.00048 \pm 0.00022 \pm 0.00032$	$0.0042 \pm 0.0013 \pm 0.0011$
16	$0.00019 \pm 0.00007 \pm 0.00015$	$0.0011 \pm 0.0005 \pm 0.0011$
17	—	$0.0004 \pm 0.0004 \pm 0.0004$
18	—	$0.00018 \pm 0.00018 \pm 0.00018$

Table 3: The charged particle multiplicity distribution of gluon jets, $n_{\rm gluon}^{\rm ch.}$, for $E_{\rm g}^{*}=8.43$ and 10.92 GeV. The data have been corrected for detector acceptance and resolution, for event selection, and for gluon jet impurity. The first uncertainty is statistical and the second systematic.

$n_{\rm gluon}^{\rm ch.}$	$P(n_{\rm gluon}^{\rm ch.})$, $E_{\rm g}^{*} = 14.24$ GeV	$P(n_{\rm gluon}^{\rm ch.})$, $E_{\rm g}^{*} = 17.72$ GeV
0	$0.0001 \pm 0.0001 \pm 0.0001$	$0.00004 \pm 0.00001 \pm 0.00004$
1	$0.0005 \pm 0.0005 \pm 0.0005$	$0.0004 \pm 0.0004 \pm 0.0004$
2	$0.0068 \pm 0.0028 \pm 0.0036$	$0.0013 \pm 0.0013 \pm 0.0013$
3	$0.0179 \pm 0.0047 \pm 0.0062$	$0.0080 \pm 0.0072 \pm 0.0057$
4	$0.0363 \pm 0.0078 \pm 0.0079$	$0.018 \pm 0.013 \pm 0.011$
5	$0.072 \pm 0.011 \pm 0.008$	$0.047 \pm 0.018 \pm 0.014$
6	$0.099 \pm 0.013 \pm 0.006$	$0.067 \pm 0.023 \pm 0.019$
7	$0.131 \pm 0.016 \pm 0.010$	$0.102 \pm 0.033 \pm 0.016$
8	$0.137 \pm 0.014 \pm 0.010$	$0.103 \pm 0.029 \pm 0.023$
9	$0.132 \pm 0.013 \pm 0.007$	$0.125 \pm 0.034 \pm 0.027$
10	$0.116 \pm 0.016 \pm 0.006$	$0.143 \pm 0.031 \pm 0.023$
11	$0.0924 \pm 0.013 \pm 0.006$	$0.128 \pm 0.029 \pm 0.024$
12	$0.067 \pm 0.012 \pm 0.006$	$0.153 \pm 0.031 \pm 0.051$
13	$0.047 \pm 0.010 \pm 0.006$	$0.054 \pm 0.020 \pm 0.046$
14	$0.025 \pm 0.006 \pm 0.007$	$0.022 \pm 0.018 \pm 0.022$
15	$0.01447 \pm 0.0020 \pm 0.0040$	$0.017 \pm 0.013 \pm 0.017$
16	$0.0051 \pm 0.0019 \pm 0.0039$	$0.010 \pm 0.010 \pm 0.009$

Table 4: The charged particle multiplicity distribution of gluon jets, $n_{\rm gluon}^{\rm ch.}$, for $E_{\rm g}^{*} = 14.24$ and 17.72 GeV. The data have been corrected for detector acceptance and resolution, for event selection, and for gluon jet impurity. The first uncertainty is statistical and the second systematic.

$E_{\rm g}^{*}$	$\langle n_{\rm gluon}^{\rm ch.} \rangle$	$F_{2,\,\rm gluon}$	$F_{3,\,\rm gluon}$
5.25	$4.803 \pm 0.030 \pm 0.047$	$0.9528 \pm 0.0030 \pm 0.0087$	$0.863 \pm 0.008 \pm 0.020$
5.98	$5.190 \pm 0.030 \pm 0.062$	$0.956 \pm 0.002 \pm 0.011$	$0.870 \pm 0.006 \pm 0.027$
6.98	$5.677 \pm 0.030 \pm 0.074$	$0.963 \pm 0.002 \pm 0.011$	$0.891 \pm 0.006 \pm 0.026$
8.43	$6.291 \pm 0.030 \pm 0.090$	$0.970 \pm 0.002 \pm 0.011$	$0.915 \pm 0.005 \pm 0.027$
10.92	$7.378 \pm 0.062 \pm 0.077$	$0.989 \pm 0.004 \pm 0.011$	$0.964 \pm 0.012 \pm 0.026$
14.24	$8.62 \pm 0.13 \pm 0.10$	$0.988 \pm 0.005 \pm 0.015$	$0.960 \pm 0.016 \pm 0.041$
17.72	$9.52 \pm 0.30 \pm 0.33$	$0.973 \pm 0.007 \pm 0.029$	$0.914 \pm 0.021 \pm 0.078$

Table 5: The mean, $\langle n_{\rm gluon}^{\rm ch.} \rangle$, and first two non-trivial normalized factorial moments, $F_{2,\,\rm gluon}$ and $F_{3,\,\rm gluon}$, of the charged particle multiplicity distribution of gluon jets. The data have been corrected for detector acceptance and resolution, for event selection, and for gluon jet impurity. The first uncertainty is statistical and the second systematic.

at the end of the perturbative shower. The theoretical results are compared to the charged particle hadron level data[3], without hadronization corrections. By hadronization correction, we mean the ratio of the parton to hadron level predictions from a QCD Monte Carlo program, e.g. Herwig. We do not apply hadronization corrections because they are model dependent. The fitted parameters therefore incorporate effects from hadronization, in addition to possible effects from approximations in the QCD expressions themselves. Our strategy is to compare the parameter values obtained from different distributions (where appropriate) to see whether they are generally similar despite hadronization, and thereby to test the global consistency of the formalism in a qualitative way.

9.1.1 3NLO perturbative expressions

A QCD analytic calculation of the energy evolution of $\langle n_{\rm gluon}^{\rm parton}\rangle$, valid to the next-to-next-to-next-to-leading order (3NLO) of perturbation theory, is presented in [35]. So far, only two tests of this expression have been performed. The first test [35] is based on two data points only: the $g_{\rm incl.}$ and $\Upsilon(3S)$-derived results shown in Fig. 8a. The second test [12] is based on these same two data points and the less direct measurements shown by the open symbols in Fig. 8a. 3NLO analytic results for $F_{2,\,\rm gluon}^{\rm parton}$ and $F_{3,\,\rm gluon}^{\rm parton}$ are presented in [36]. So far, there have been no experimental tests of the energy evolution of these expressions.

The solid curve in Fig. 8a shows the result of a two parameter χ^2 fit of the 3NLO expression for $\langle n_{\rm gluon}^{\rm parton}\rangle$ to the $\langle n_{\rm gluon}^{\rm ch.}\rangle$ data. The fit is performed assuming $n_F = 5$, where n_F is the number of active quark flavors in the perturbative stage of an event. Essentially identical curves are obtained if $n_F = 3$ or 4 (see below) is used instead. The fitted data are the seven measurements of $\langle n_{\rm gluon}^{\rm ch.}\rangle$ from the present study (see Table 5) and the $g_{\rm incl.}$ and $\Upsilon(3S)$ results shown in Fig. 8a. The fits are performed using statistical uncertainties only to determine the χ^2. The fitted parameters are the QCD scale parameter Λ and an overall normalization constant K (see [35]). Note that Λ is strongly correlated with $\Lambda_{\overline{\rm MS}}$ [37] but is not necessarily the same. Note also that there is an ambiguity in the appropriate value to use for n_F because c and b quarks are rarely produced in the perturbative evolution of jets at LEP. The fitted parameter values and corresponding χ^2 results are listed in the top portion of Table 6. The results are given for $n_F = 3$, 4 and 5. The systematic uncertainties attributed to the parameters are defined by adding the following contributions in quadrature: (1) the uncertainty of the fitted parameters returned by the fitting routine when the total uncertainties of the data are used to perform the fit, rather than the statistical uncertainties only (note: point-to-point systematic uncertainties are treated as uncorrelated); (2) the difference between the results of the standard fit and those found by fitting only the $\langle n_{\rm gluon}^{\rm ch.}\rangle$ data of Table 5 (i.e. excluding the $g_{\rm incl.}$ and $\Upsilon(3S)$ measurements).

From Fig. 8a and Table 6, it is seen that the 3NLO expression provides a good description of the $\langle n_{\rm gluon}^{\rm ch.}\rangle$ measurements, i.e. $\chi^2/{\rm d.o.f.} = 0.74$ for $n_F = 5$, with slightly higher χ^2 for $n_F = 3$ and 4. The result $\Lambda = 0.296 \pm 0.037\,({\rm stat.+syst.})$ GeV we find for $n_F = 5$ is much more similar to the corresponding quark jet result, $\Lambda = 0.190 \pm 0.032\,({\rm stat.})$ GeV [12], than to the value $\Lambda = 0.60 \pm 0.06\,({\rm stat.})$ GeV found previously [12] ("stat.+syst." means the statistical and

[3]The issue of how this comparison differs from one based on both charged and neutral particles at the hadron level is addressed in Sect. 9.1.1.

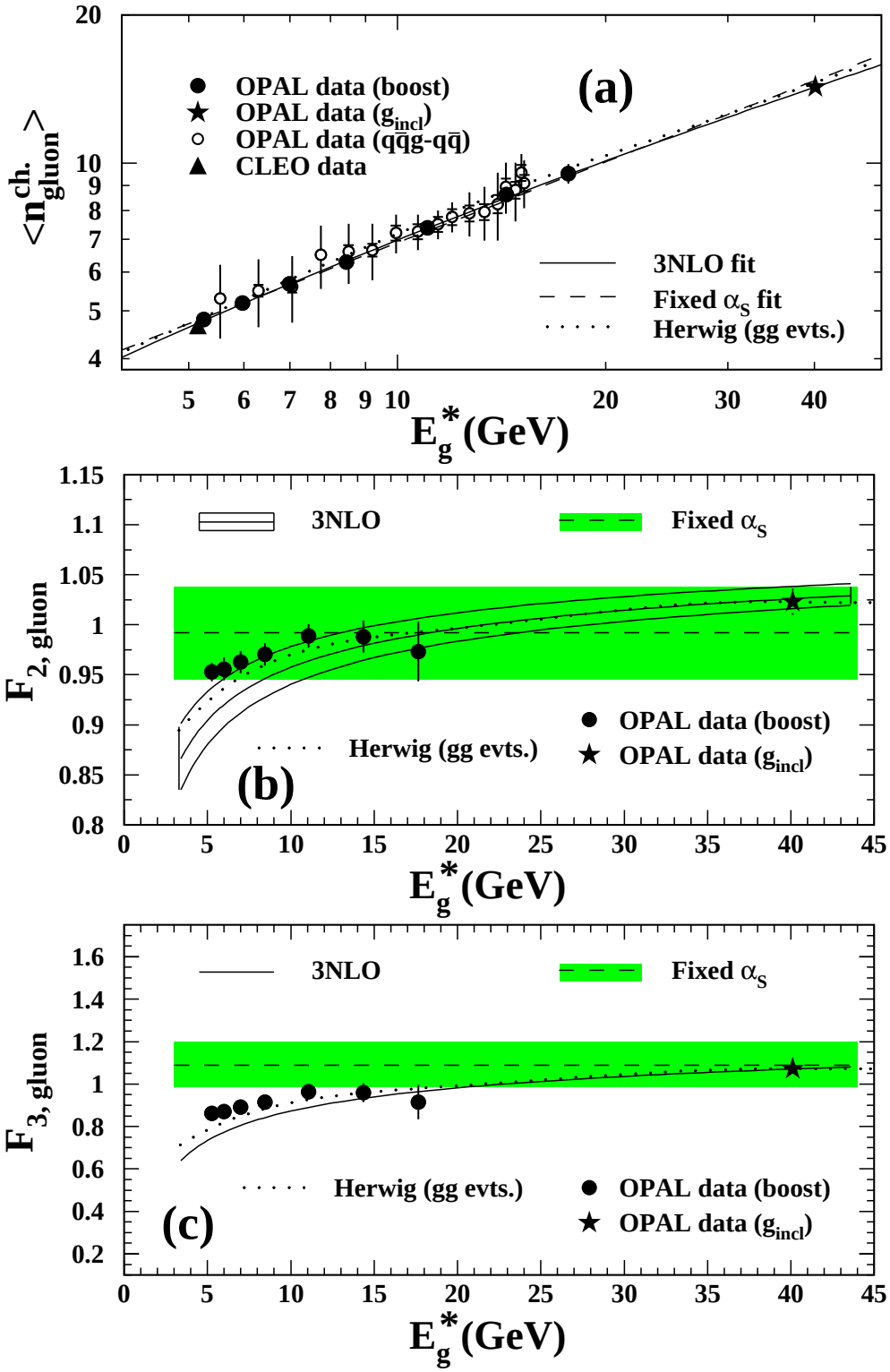

Figure 8: (a) The mean charged particle multiplicity value of gluon jets, $\langle n_{\rm gluon}^{\rm ch.} \rangle$, as a function of the gluon jet energy $E_{\rm g}^{*}$. The data have been corrected for detector acceptance and resolution, for event selection, and for gluon jet impurity. The total uncertainties are shown by the vertical lines, with the statistical component delimited by small horizontal lines. (b,c) The corresponding results for the two lowest non-trivial normalized factorial moments, $F_{2,\,\rm gluon}$ and $F_{3,\,\rm gluon}$. The data are presented in comparison to the result of QCD analytic calculations, and to the Herwig Monte Carlo at the hadron level.

	n_F	Λ (GeV)	K	χ^2/d.o.f.
$\langle n^{\rm ch.}_{\rm gluon}\rangle$	3	$0.470 \pm 0.027 \pm 0.050$	$0.1366 \pm 0.0047 \pm 0.0084$	6.2/7
	4	$0.385 \pm 0.024 \pm 0.046$	$0.1164 \pm 0.0042 \pm 0.0080$	5.6/7
	5	$0.296 \pm 0.019 \pm 0.038$	$0.0986 \pm 0.0037 \pm 0.0073$	5.2/7
$F_{2,\,\rm gluon}$	3	$0.166 \pm 0.012 \pm 0.049$	—	8.7/2
	4	$0.143 \pm 0.009 \pm 0.042$	—	8.2/2
	5	$0.114 \pm 0.009 \pm 0.032$	—	8.2/2
$F_{3,\,\rm gluon}$	3	$0.051 \pm 0.004 \pm 0.016$	—	8.4/2
	4	$0.040 \pm 0.003 \pm 0.013$	—	8.4/2
	5	$0.029 \pm 0.002 \pm 0.011$	—	8.1/2

Table 6: Results of fits of the 3NLO expressions for $\langle n^{\rm ch.}_{\rm gluon}\rangle$ [35], $F_{2,\,\rm gluon}$ and $F_{3,\,\rm gluon}$ [36] to our data. The χ^2 values are based on the statistical uncertainties of the data points. The first uncertainty is statistical and the second systematic.

systematic terms have been added in quadrature). Our data therefore provide a much improved demonstration of the consistency of the 3NLO expressions for the scale dependence of unbiased quark and gluon jet multiplicities than previously available.

The solid curves in Figs. 8b and c show the corresponding results of fits of the 3NLO expressions for $F^{\rm parton}_{2,\,\rm gluon}$ and $F^{\rm parton}_{3,\,\rm gluon}$ to the data. We note that the hadronization corrections predicted for $F_{2,\,\rm gluon}$ and $F_{3,\,\rm gluon}$ (from Herwig) exhibit a significant dependence on energy, especially for $E^*_{\rm g} \lesssim 12$ GeV. The hadronization correction predicted for $F_{2,\,\rm gluon}$ changes by about 19% for $5 \leq E^*_{\rm g} \leq 12$ GeV, for example (from 0.70 to 0.83), compared to about 12% for $12 \leq E^*_{\rm g} \leq 40$ GeV (from 0.83 to 0.93). For $F_{3,\,\rm gluon}$, the results are 71% (from 0.34 to 0.58) and 43% (from 0.58 to 0.83), respectively. (In comparison, the hadronization correction predicted for the $\langle n^{\rm ch.}_{\rm gluon}\rangle$ distribution in Fig. 8a changes by only about 10% and 6% over these intervals, corresponding to corrections of 0.39, 0.35 and 0.33 at 5, 12 and 40 GeV.) Therefore, the fits of the 3NLO expressions for $F^{\rm parton}_{2,\,\rm gluon}$ and $F^{\rm parton}_{3,\,\rm gluon}$ shown in Figs. 8b and c are restricted to the three data points with $E^*_{\rm g} > 12$ GeV, i.e. the data at 14.24, 17.72 and 40.1 GeV. The results of the fits are listed in the central and bottom portions of Table 6. Since $F^{\rm parton}_{2,\,\rm gluon}$ and $F^{\rm parton}_{3,\,\rm gluon}$ are normalized moments, they are independent of an overall normalization factor, i.e. Λ is the only free parameter. The χ^2/d.o.f. of these fits are seen to be quite large (Table 6): this is because the statistical uncertainties are relatively small and the $F_{2,\,\rm gluon}$ and $F_{3,\,\rm gluon}$ measurements at 17.72 GeV are low compared to the corresponding data at 14.24 GeV and 40.1 GeV (see Figs. 8b and c). Note, however, that the $F_{2,\,\rm gluon}$ and $F_{3,\,\rm gluon}$ measurements at 17.72 GeV have large systematic uncertainties and that the fitted curves in Figs. 8b and c describe the energy evolution of $F_{2,\,\rm gluon}$ and $F_{3,\,\rm gluon}$ from 14 to 40 GeV quite well if the total uncertainties of the measurements are considered. In contrast, the 3NLO curves lie below the data at smaller energies.

The systematic uncertainties attributed to the Λ values found from fitting the $F_{2,\,\rm gluon}$ and $F_{3,\,\rm gluon}$ data (Table 6) are defined by adding the following contributions in quadrature: (1) the uncertainty of the fitted parameters returned by the fitting routine when the total uncertainties of the data are used to perform the fit, rather than the statistical uncertainties only; (2) the difference between the standard results and those found by repeating the fits including the data

at 10.92 GeV; (3) the difference between the standard results and those found by repeating the fits excluding the $g_{\rm incl.}$ measurements at 40.1 GeV. The open band in Fig. 8b shows the uncertainty of the 3NLO curve, defined by increasing or decreasing Λ by one standard deviation of its total uncertainty as determined using the $F_{2,\,\rm gluon}$ data. The corresponding one standard deviation band for the $F_{3,\,\rm gluon}$ curve is too small to be visible.

The fitted results for Λ from $F_{2,\,\rm gluon}$ and $F_{3,\,\rm gluon}$, viz. 0.114 and 0.029 GeV (for $n_F = 5$), differ from each other and also from the result $\Lambda = 0.296$ GeV found from the fit to the $\langle n^{\rm ch.}_{\rm gluon}\rangle$ data (Table 6). These differences may be a consequence of the different energy dependence of the hadronization corrections for the three distributions, predicted to be more substantial for $F_{3,\,\rm gluon}$ than for $F_{2,\,\rm gluon}$, and for $F_{2,\,\rm gluon}$ than for $\langle n^{\rm ch.}_{\rm gluon}\rangle$, as discussed above. For purposes of comparison, it is interesting to express these Λ results in terms of the coupling strength at the $\rm Z^0$ pole, $\alpha_S\,(m_{\rm Z})$.[4] The fitted Λ results for $\langle n^{\rm ch.}_{\rm gluon}\rangle$, $F_{2,\,\rm gluon}$ and $F_{3,\,\rm gluon}$ correspond to $\alpha_S\,(m_{\rm Z}) = 0.123 \pm 0.002$, 0.107 ± 0.003 and 0.090 ± 0.002, respectively, where the statistical and systematic uncertainties have been added in quadrature. Since Λ in the 3NLO calculations does not correspond to $\Lambda_{\overline{\rm MS}}$, these values of $\alpha_S\,(m_{\rm Z})$ cannot be compared directly to the world average $\alpha_S\,(m_{\rm Z}) = 0.117 \pm 0.002$ [39]. Furthermore they cannot be compared directly to each other since the effects of hadronization are different for the $\langle n^{\rm ch.}_{\rm gluon}\rangle$, $F_{2,\,\rm gluon}$ and $F_{3,\,\rm gluon}$ distributions as noted above. Nonetheless, the three α_S results are globally similar to each other and to the world average value, i.e. they are more similar to $\alpha_S \sim 0.1$ than to e.g. $\alpha_S \sim 0.01$ or 1.0. It is notable that the 3NLO results for $F^{\rm parton}_{2,\,\rm gluon}$ and $F^{\rm parton}_{3,\,\rm gluon}$ found using these qualitatively sensible values ($\alpha_S \sim 0.1$) are much more similar to the experimental measurements in Figs. 8b and c than to the leading order QCD predictions of 4/3 and 9/4, respectively [36]. In this general sense, the 3NLO calculations provide a qualitatively consistent and successful description of the gluon jet multiplicity data, at least for $E^*_{\rm g} \gtrsim 14$ GeV.

We note that most of the multiplicity in high energy jets is generated by hard, virtual gluons, common to both charged and neutral particles at the hadron level. As a consequence, the shapes of the multiplicity distributions of neutral and charged hadrons are expected to be very similar, so that it makes no difference if parton level expressions are compared to charged particle data only (as is done here) or to data including neutral hadrons as well. The shapes of the multiplicity distributions of charged and neutral particles at the hadron level can differ, however, because of resonance decays which introduce correlations, e.g. in $\pi^0 \to \gamma\gamma$ decays which produce most of the stable neutral particles at the hadron level. Using hadron level Herwig events, we verified that the fitted results for Λ from the $\langle n_{\rm gluon}\rangle$, $F_{2,\,\rm gluon}$ and $F_{3,\,\rm gluon}$ distributions are almost identical if neutral particles at the hadron level are used to define the multiplicity distributions, rather than charged particles, as long as the π^0 is declared stable. The results for the normalization constant K in the 3NLO expression for $\langle n^{\rm parton}_{\rm gluon}\rangle$ differ in the fits for neutral and charged hadrons, however, because the mean numbers of charged and neutral hadrons are not the same.

9.1.2 Fixed α_S expressions

Analytic expressions for $\langle n^{\rm parton}_{\rm gluon}\rangle$, $F^{\rm parton}_{2,\,\rm gluon}$ and $F^{\rm parton}_{3,\,\rm gluon}$ have also been derived assuming a fixed value of α_S [40, 41]. By assuming α_S is fixed, the QCD evolution equations for multiplicity

[4] We relate Λ to $\alpha_S\,(m_{\rm Z})$ using the two-loop formula given, for example, by (75) in [38].

n_F	α_S	$r_{\mathrm{g/q}}$
3	$0.293 \pm 0.016 \pm 0.035$	$1.718 \pm 0.014 \pm 0.040$
4	$0.297 \pm 0.017 \pm 0.036$	$1.697 \pm 0.014 \pm 0.041$
5	$0.301 \pm 0.017 \pm 0.036$	$1.679 \pm 0.014 \pm 0.042$

Table 7: Results for α_S and $r_{\mathrm{g/q}}$ from fitting the fixed α_S expression for $\langle n^{\mathrm{ch.}}_{\mathrm{gluon}} \rangle$ [40] to our data. Note that the energy scale associated with these results is ambiguous (see text). The first uncertainty is statistical and the second systematic.

can be solved exactly, without recourse to a perturbative approximation (for a recent review, see [38]). The solutions based on fixed α_S therefore more completely incorporate such higher order effects as energy conservation than do the 3NLO calculations. On the other hand, the fixed α_S results do not account for the change in α_S with scale.

The dashed curve in Fig. 8a shows the result of a fit of the fixed α_S expression for gluon jet multiplicity [40],

$$\langle n^{\mathrm{parton}}_{\mathrm{gluon}} \rangle = \left(\frac{E^*_{\mathrm{g}}}{Q_0} \right)^{\gamma} \quad , \tag{6}$$

to the $\langle n^{\mathrm{ch.}}_{\mathrm{gluon}} \rangle$ data. The fitted data are the seven measurements of $\langle n^{\mathrm{ch.}}_{\mathrm{gluon}} \rangle$ in Table 5 and the $\mathrm{g_{incl.}}$ and $\Upsilon(3S)$ results in Fig. 8a. The fitted parameters are γ and Q_0. Q_0 is a cut-off for soft gluon radiation while γ is the so-called anomalous dimension of QCD, which takes into account perturbative corrections to the coupling strength. The results are $\gamma = 0.548 \pm 0.009\,(\mathrm{stat.}) \pm 0.028\,(\mathrm{syst,})$ and $Q_0 = 0.295 \pm 0.017\,(\mathrm{stat.}) \pm 0.053\,(\mathrm{syst.})$ GeV, where the systematic uncertainties are evaluated as explained for the 3NLO fit to $\langle n^{\mathrm{ch.}}_{\mathrm{gluon}} \rangle$ in Sect. 9.1.1. The χ^2/d.o.f. is 21/7, larger than the result found using the 3NLO expression (see Table 6). The fixed α_S calculation provides a reasonable description of the data within the total uncertainties of the measurements, however.

Assuming a specific value for n_F, i.e. $n_F = 3$, 4 or 5, our result for γ can be used to derive values for α_S and $r_{\mathrm{g/q}}$, where $r_{\mathrm{g/q}}$ is the ratio between the mean particle multiplicities of gluon and quark jets:

$$r_{\mathrm{g/q}} = \frac{\langle n_{\mathrm{gluon}} \rangle}{\langle n_{\mathrm{quark}} \rangle} \quad , \tag{7}$$

(see e.g. (120) and (121) in [38] and the ensuing text). The results are given in Table 7. Note that since α_S is constant in this formalism, as is $r_{\mathrm{g/q}}$, there is an ambiguity in the energy scale of these results. This ambiguity may partly explain the large value $\alpha_S \sim 0.3$ we obtain for the coupling strength. In addition, the assumption that α_S is constant is not entirely realistic for the energy range of our study. For these reasons, the results for α_S in Table 7 are not very meaningful. They are included for completeness only. In contrast, the results for $r_{\mathrm{g/q}}$ are found to be only weakly dependent on the energy scale and on the corresponding variation in α_S [40] and thus have more significance. For the multiplicity ratio, we obtain $r_{\mathrm{g/q}} \approx 1.7$. This result is discussed further in Sect. 9.1.3.

The fixed α_S expressions for $F_{2,\,\mathrm{gluon}}$ and $F_{3,\,\mathrm{gluon}}$ [41] depend on n_F and γ. Because these expressions are complicated, we do not fit them to data but instead evaluate them using the

result for γ found by fitting the $\langle n_{\rm gluon}^{\rm ch.}\rangle$ measurements (cf. the dashed curve Fig. 8a). The results, evaluated for $n_F = 5$, are shown by the dashed lines in Figs. 8b and c. Almost identical results are obtained for $n_F = 3$ or 4. The shaded regions indicate the total uncertainties, defined by repeating the study after increasing or decreasing γ by its total uncertainty (see above). The fixed α_S prediction for $F_{2,\,\rm gluon}$ (Fig. 8b) is seen to accommodate the data within its fairly large uncertainty. The corresponding result for $F_{3,\,\rm gluon}$ (Fig. 8c) agrees with the data point at 40.1 GeV but lies above the measurements at lower energies.

9.1.3 Comparison to quark jets

It is interesting to compare the results of Table 5 to corresponding measurements for quark jets. This allows further tests of QCD calculations.

The particle multiplicity of unbiased quark jets has been measured at many scales. For our study, we choose results from the ARGUS [42], JADE [43] and HRS [44] experiments at c.m. energies of 10.5, 12.0 and 29.0 GeV, and from the TASSO [45] experiment at 14.0, 22.0 and 34.5 GeV. We select these data because the quark jet energies, given by half the c.m. values, correspond to the mean energies $\langle E_{\rm g}^*\rangle$ of our gluon jets, with the exception of the sample with $\langle E_{\rm g}^*\rangle = 8.43$ GeV (see Table 1).

Fig. 9a shows the ratio of the mean charged particle multiplicities between gluon and quark jets, $r_{\rm g/q}$ (see eq. (7)), for the six energies for which the quark jet scales correspond to our gluon data. The analogous results for F_2 and F_3, denoted $F_2^{\rm g/q}$ and $F_3^{\rm g/q}$, are shown in Figs. 9b and c. The latter results are limited to energies of 6.98, 10.92, 14.24 and 17.72 GeV because information about higher moments of the quark jet (hemisphere) multiplicity distributions is not available for the other energies. Figs. 9a–c include our previous measurements at 40.1 GeV [8,9]. Fig. 9a also includes the result for $r_{\rm g/q}$ we obtain by dividing the CLEO [5] and ARGUS [42] measurements of unbiased gluon and quark multiplicities, respectively. The quark jet data have in all cases been corrected for the small differences in energy between the gluon and corresponding quark jet samples, and for the presence of c and b flavored jets. The reason for this latter correction is that the theoretical results for $r_{\rm g/q}$ assume massless quarks. The corrections were determined using bin-by-bin factors derived from Herwig. The total corrections for the mean multiplicities of quark jets are about 10% and are approximately independent of energy. The corresponding corrections for the F_2 and F_3 distributions of quark jets are about 1% and 3%, respectively. Very similar results are obtained using Jetset and Ariadne.

The dotted and dash-dotted curves in Fig. 9a show the Herwig predictions for $r_{\rm g/q}$ at the hadron and parton levels. It is seen that the parton and hadron level results are very similar, even for small energies $E_{\rm g}^* \sim 5$ GeV. We conclude that hadronization effects are small for $r_{\rm g/q}$. Comparing the dotted and dash-dotted curves in Figs. 9b and c, it is seen that the hadronization corrections predicted for $F_2^{\rm g/q}$ and $F_3^{\rm g/q}$ are fairly large and have a significant dependence on energy. The hadronization correction of $F_2^{\rm g/q}$ is predicted to be about 20% for $E_{\rm g}^* = 7$ GeV, decreasing to about 12% at 14 GeV and 6% at 40 GeV. The corresponding values for $F_3^{\rm g/q}$ are 50%, 25% and 12%.

A 3NLO analytic expression for $r_{\rm g/q}$ is presented in [46]. Λ is the only free parameter in this expression. The open band in Fig. 9a shows the results we obtain by evaluating this expression

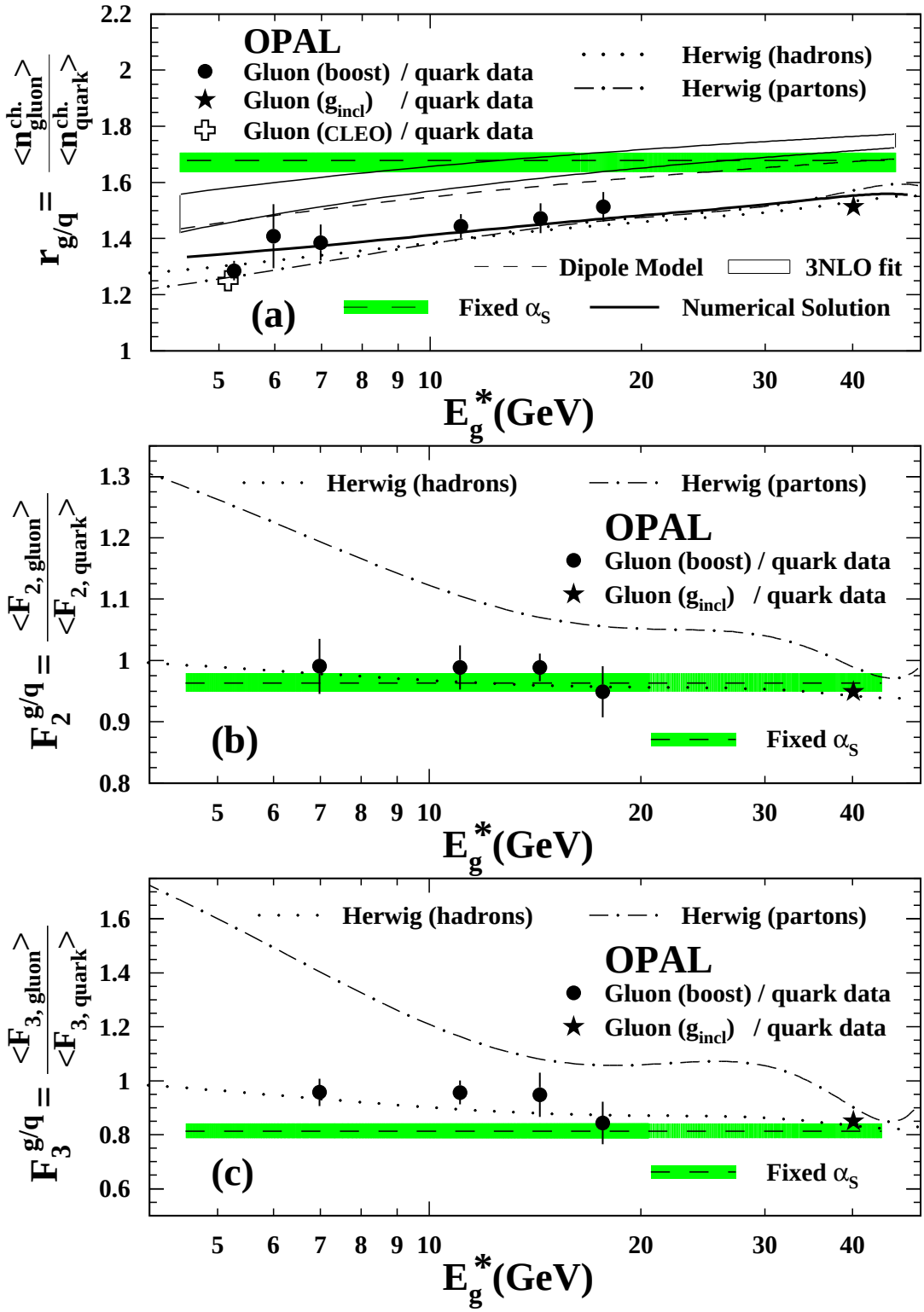

Figure 9: (a) The ratio between the mean charged particle multiplicities of unbiased gluon and uds flavored quark jets, $r_{g/q}$, as a function of jet energy. The data have been corrected for detector acceptance and resolution, for event selection, and for gluon jet impurity. The vertical lines indicate the total uncertainties. Statistical uncertainties are too small to be visible. (b,c) The corresponding results for the factorial moments of the multiplicity distributions, F_2 and F_3. The data are presented in comparison to the results of QCD calculations, and to the Herwig Monte Carlo at the hadron and parton levels.

using $n_F = 5$. The lower edge of the band corresponds to $\Lambda = 0.296$ GeV, i.e. the value from Sect. 9.1.1 from the fit of the 3NLO expression for $\langle n^{\rm ch.}_{\rm gluon} \rangle$. The upper edge shows the result using the corresponding value [12] for unbiased quark jet multiplicity, $\Lambda = 0.190$ GeV. The 3NLO prediction is seen to lie 15–20% above the data. We also tried to fit the 3NLO expression for $r_{\rm g/q}$ to the data in Fig. 9a. We find that the theoretical expression is unable to simultaneously provide a good description of the data at both low and high energies. A fit of the three highest energy points (14.24, 17.72 and 40.1 GeV) yields $\Lambda = 1.07 \pm 0.16\,({\rm stat.})$ GeV, with a χ^2/d.o.f. of 6.1/2. This value of Λ is considerably larger than that found from the fit to the $\langle n^{\rm ch.}_{\rm gluon} \rangle$ data, mentioned above. In contrast to $r_{\rm g/q}$, 3NLO perturbative expressions for $F_2^{\rm g/q}$ and $F_3^{\rm g/q}$ are not yet available.

The long-dashed line in Fig. 9a shows the prediction of the fixed α_S calculation for $r_{\rm g/q}$, assuming $n_F = 5$ (see Table 7). The shaded band corresponds to the one standard deviation total uncertainty for this quantity (Table 7). The corresponding results for $F_2^{\rm g/q}$ and $F_3^{\rm g/q}$ are shown in Figs. 9b and c. The fixed α_S result for $F_2^{\rm g/q}$ is determined by taking the ratio of the F_2 expressions for gluon and quark jets [41], using $\alpha_S = 0.301$ from Table 7. The fixed α_S result for $F_3^{\rm g/q}$ is determined in an analogous manner. The overall description of $r_{\rm g/q}$ by the fixed α_S calculation (Fig. 9a) is seen to be similar to that of the 3NLO result, being in somewhat better agreement with the data at high energies ($E^*_{\rm g} \approx 40$ GeV) and in worse agreement at low energies ($E^*_{\rm g} \lesssim 10$ GeV). The fixed α_S prediction for $F_2^{\rm g/q}$ (Fig. 9b) is in good agreement with the measurements, while the prediction for $F_3^{\rm g/q}$ (Fig. 9c) is in good agreement for $E^*_{\rm g} \gtrsim 14$ GeV. Given the significant hadronization corrections predicted for these last two distributions, discussed above, the good agreement between the data and fixed α_S results in Figs. 9b and c may be somewhat accidental.

A theoretical result for $r_{\rm g/q}$ has also been determined in the context of the dipole model [48]. This result is shown by the short-dashed curve in Fig. 9a. The dipole model prediction is seen to lie above the data, but to be in somewhat better agreement with the measurements than the 3NLO result.

Finally, we include in Fig. 9a a theoretical result [47] for $r_{\rm g/q}$ based on a numerical, rather than an analytic, solution of the QCD evolution equations for multiplicity. This result is shown by the solid line. Like the fixed α_S solution, the numerical solution is "exact" in the sense that it is not based on a perturbative approximation. The numerical result allows better accounting of energy conservation effects and phase space limits than the analytic results, and incorporates a running value for α_S (see [38,47] for further discussion). The value of Λ used for the numerical calculation is 0.50 GeV, determined from a fit to measurements of jet rates in Z^0 decays [47]. The numerical calculation is seen to provide a much improved description of the $r_{\rm g/q}$ data compared to the 3NLO or fixed α_S expressions. This suggests that much of the discrepancy between the data and analytic results in Fig. 9 is a consequence of technical difficulties in the calculations (the inclusion of energy conservation, etc.), rather than shortcomings of QCD. Similar conclusions are presented in [38].

bin in x_E^*	$1/N\,(\mathrm{d}n^{\mathrm{ch.}}_{\mathrm{gluon}}/\mathrm{d}x_E^*)$, $E_{\mathrm{g}}^* = 14.24$ GeV	$1/N\,(\mathrm{d}n^{\mathrm{ch.}}_{\mathrm{gluon}}/\mathrm{d}x_E^*)$, $E_{\mathrm{g}}^* = 17.72$ GeV
0.00–0.01	$4.9 \pm 1.2 \pm 4.7$	$27.1 \pm 5.3 \pm 7.3$
0.01–0.02	$104.7 \pm 4.3 \pm 4.9$	$155 \pm 13 \pm 17$
0.02–0.03	$131.4 \pm 5.0 \pm 7.2$	$128 \pm 11 \pm 17$
0.03–0.04	$93.4 \pm 6.1 \pm 5.8$	$110 \pm 9 \pm 16$
0.04–0.05	$89.0 \pm 3.8 \pm 6.6$	$106 \pm 8 \pm 25$
0.05–0.06	$61.8 \pm 4.0 \pm 8.3$	$83 \pm 8 \pm 21$
0.06–0.07	$55.4 \pm 4.0 \pm 7.1$	$76 \pm 7 \pm 16$
0.07–0.08	$54.7 \pm 3.2 \pm 5.6$	$46 \pm 6 \pm 15$
0.08–0.09	$41.1 \pm 2.7 \pm 4.7$	$50 \pm 6 \pm 14$
0.09–0.10	$33.9 \pm 2.9 \pm 3.5$	$48 \pm 5 \pm 18$
0.10–0.12	$27.0 \pm 1.7 \pm 3.7$	$24 \pm 3 \pm 15$
0.12–0.14	$15.9 \pm 1.6 \pm 2.8$	$18.2 \pm 2.4 \pm 6.0$
0.14–0.16	$14.7 \pm 1.0 \pm 3.0$	$11.1 \pm 2.1 \pm 2.9$
0.16–0.18	$10.2 \pm 1.0 \pm 2.0$	$10.5 \pm 2.0 \pm 3.3$
0.18–0.20	$7.6 \pm 0.7 \pm 1.2$	$5.4 \pm 1.5 \pm 4.3$
0.20–0.25	$4.75 \pm 0.40 \pm 0.88$	$4.2 \pm 0.7 \pm 3.1$
0.25–0.30	$1.96 \pm 0.27 \pm 0.66$	$2.6 \pm 0.6 \pm 1.3$
0.30–0.40	$0.66 \pm 0.09 \pm 0.50$	$0.71 \pm 0.17 \pm 0.71$
0.40–0.50	$0.19 \pm 0.06 \pm 0.14$	$0.14 \pm 0.06 \pm 0.14$
0.50–0.60	$0.160 \pm 0.082 \pm 0.086$	$0.029 \pm 0.013 \pm 0.029$
0.60–0.80	$0.014 \pm 0.009 \pm 0.014$	$0.012 \pm 0.012 \pm 0.012$
0.80–1.00	$0.0002 \pm 0.0002 \pm 0.0002$	—

Table 8: The charged particle fragmentation function of gluon jets, $1/N\,(\mathrm{d}n^{\mathrm{ch.}}_{\mathrm{gluon}}/\mathrm{d}x_E^*)$, for $E_{\mathrm{g}}^* = 14.24$ and 17.72 GeV. The data have been corrected for detector acceptance and resolution, for event selection, and for gluon jet impurity. The first uncertainty is statistical and the second systematic.

9.2 Fragmentation functions

We next turn to a discussion of the gluon jet fragmentation function. Our results for the corrected fragmentation functions of unbiased gluon jets at $E_{\mathrm{g}}^* = 14.24$ and 17.72 GeV are presented in Figs. 5f and g, and again in Fig. 10. Numerical values for these data are given in Table 8.

Unlike multiplicity, the shape of fragmentation functions is not presently calculable. If the shape of a fragmentation function is known at a particular scale, the DGLAP [49] evolution equations can be used to predict the shape at a different scale, however. Since gluon jets can evolve through splitting to a quark-antiquark pair, as well as through gluon emission, the evolution of the gluon jet fragmentation function depends on the quark jet fragmentation function, in addition to that of the gluon. In [9], we presented results for the unbiased gluon jet fragmentation function at 40.1 GeV. Measurements of unbiased, flavor-separated (uds, c and b) quark jet fragmentation functions at 45.6 GeV are presented in [50]. By applying the DGLAP equations to these measurements, we can obtain QCD predictions for the gluon jet

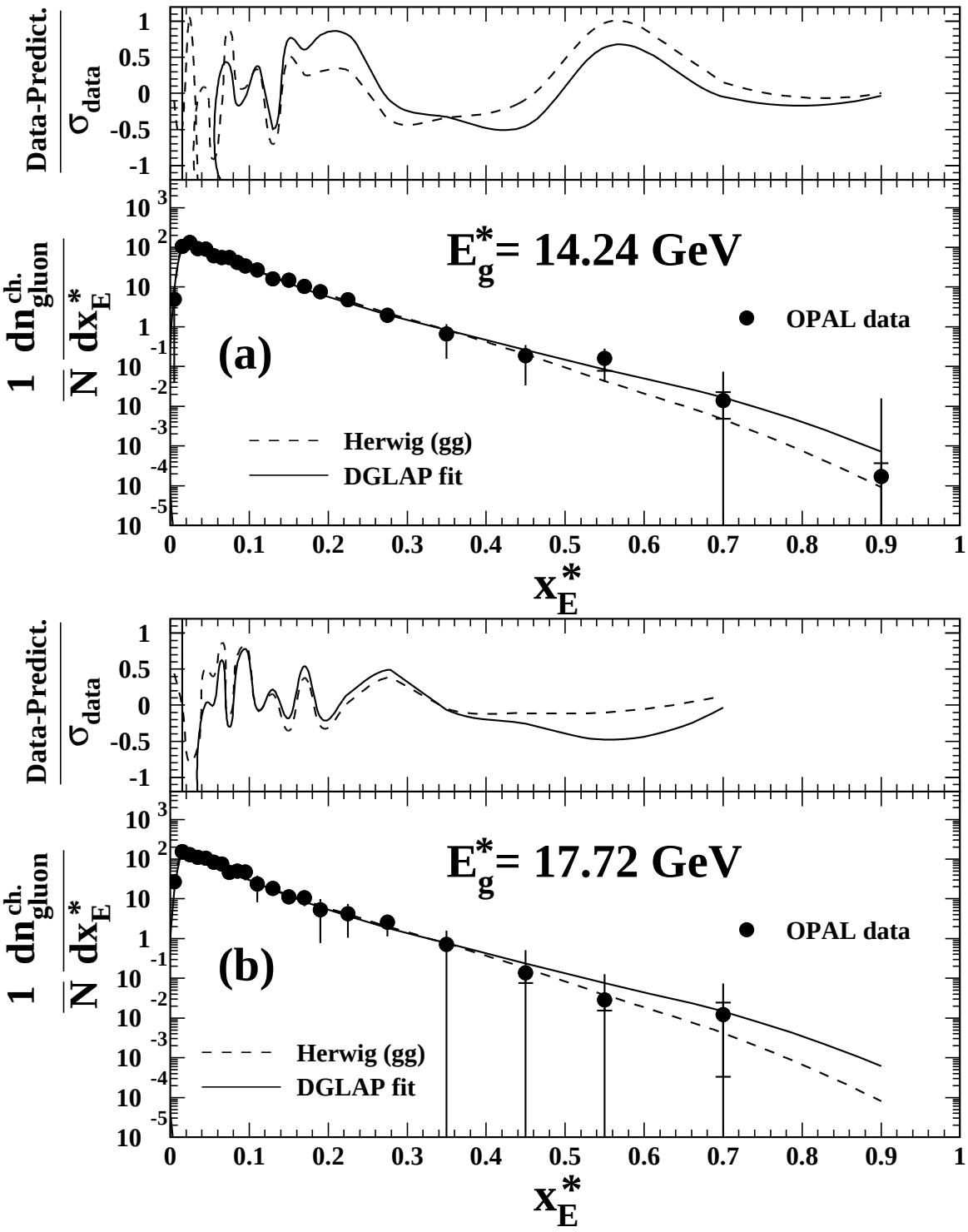

Figure 10: The charged particle fragmentation function of gluon jets, $1/N\,(\mathrm{d}n^{\mathrm{ch.}}_{\mathrm{gluon}}/\mathrm{d}x^*_E)$, for (a) $E^*_{\mathrm{g}} = 14.24$ and (b) 17.72 GeV. The data have been corrected for detector acceptance and resolution, for event selection, and for gluon jet impurity. The total uncertainties are shown by the vertical lines, with the statistical component delimited by small horizontal lines. The data are presented in comparison to a QCD prediction based on DGLAP evolution of unbiased gluon and quark jet fragmentation functions measured at 40.1 and 45.6 GeV, respectively, and to the Herwig Monte Carlo at the hadron level. The small figures above each distribution show the differences between the QCD and Herwig curves relative to the data, in units of the total experimental uncertainties.

	a	b	c	d
uds	0.2589 ± 0.0074	-2.949 ± 0.016	0.859 ± 0.029	0.2967 ± 0.0020
c	0.546 ± 0.035	-2.67 ± 0.016	2.37 ± 0.21	0.2651 ± 0.0029
b	0.3284 ± 0.0016	-3.042 ± 0.0016	2.6055 ± 0.015	0.31805 ± 0.00017
g	0.0891 ± 0.0047	-3.84 ± 0.012	2.62 ± 0.26	0.4144 ± 0.0023

Table 9: Parameter values used to describe the fragmentation functions of unbiased quark and gluon jets at 45.6 GeV (see eq. (8)). The uncertainties are statistical.

fragmentation function at the scales of the present study.

We note that the quark jet data in [50] are presented in terms of the scaled charged particle three-momenta $x_p = 2p/E_{\rm c.m.}$ (with p the particle three-momentum), rather than $x_E = 2E/E_{\rm c.m.}$ (with E the particle energy), and that x_p and x_E differ for small particle energies (or momenta). Using detector level events, we find that fragmentation functions defined using x_p differ from those defined by x_E by about 1% for x_p (or x_E) $= 0.10$, and by about 2.5% for x_p (or x_E) $= 0.05$, for example.

The fragmentation functions of gluon and quark jets are parametrized at a reference scale $\sqrt{s_0}$ using the empirical formula [51]

$$F^i(x_E; \sqrt{s_0}) = a_i \, x_E^{b_i} \, (1 - x_E)^{c_i} \exp\{-d_i \, \ln^2 x_E\} \quad , \tag{8}$$

where $i =$ g, uds, c, or b. To determine the parameters a, b, c and d for quark jets, we fit eq. (8) to the measurements in [50], i.e. we choose $\sqrt{s_0} = 45.6$ GeV. To determine the parameters for gluon jets at this same scale, we first apply an energy correction to the 40.1 GeV data. The corrections are performed using bin-by-bin factors determined from Herwig and have a typical size of about 5%. Eq. (8) is then fitted to the corrected gluon jet data to determine the parametrization of the gluon jet fragmentation function at 45.6 GeV. The fits are performed using the statistical uncertainties of the data and provide good descriptions of the measurements to within their overall uncertainties. The results we obtain are listed in Table 9.

We then use the program Evolve [52] to determine the QCD prediction for the gluon jet fragmentation function at other scales. Evolve is based on next-to-leading order expressions (see [53]) determined in the $\overline{\rm MS}$ renormalization scheme. We determine the predictions of the program for the gluon jet fragmentation functions at 14.24 and 17.72 GeV, and calculate the global χ^2 with respect to our corresponding measurements. The global χ^2 is defined by the sum of the χ^2 from the two energies. The χ^2 are calculated using the statistical uncertainties of the data. To avoid the edges of the distribution where there are theoretical ambiguities [52], the global χ^2 is evaluated in the x_E range from 0.10 to 0.80 only. Note this excludes the small x_E region where fragmentation functions defined using x_E or x_p differ by more than 1%.

We fit the value of $\alpha_S(m_{\rm Z})$ in Evolve to minimize the global χ^2. The result is $\alpha_S(m_{\rm Z}) = 0.128 \pm 0.008\,({\rm stat.}) \pm 0.015\,({\rm syst.})$. The χ^2/d.o.f. of the fit, based on statistical uncertainties, is 40.5/21. The systematic uncertainty is defined by adding the following contributions in quadrature: (1) the uncertainty returned by the fitting routine when the total uncertainties of the data are used to perform the fit, rather than the statistical uncertainties only; (2) the

difference with respect to the standard result if the range $0.05 \leq x_E \leq 0.80$ is used to define the global χ^2, rather than $0.10 \leq x_E \leq 0.80$. The systematic uncertainty from the second term is about 50% larger than that from the first term. While our result for $\alpha_S\,(m_{\rm Z})$ is not competitive with other measurements (see e.g. [39]), it does provide a unique consistency test of QCD since it is the first determination of $\alpha_S\,(m_{\rm Z})$ in the $\overline{\rm MS}$ scheme based on unbiased gluon jets. The result of the fit is shown in comparison to the data in Figs. 10a and b. The difference plots in the top portions of these figures show the differences between the data and fit in units of the total experimental uncertainties. The fit is seen to provide a good description of the measurements.

10 Summary

In this paper, we present the first experimental study to use the jet boost algorithm, a method based on the QCD dipole model to extract properties of unbiased gluon jets from $\rm e^+e^- \to q\overline{q}g$ events. We test the jet boost algorithm using the Herwig Monte Carlo QCD simulation program, comparing the results of this method to those derived from unbiased gluon jets defined by hemispheres of inclusive gg events from a color singlet point source. We examine two distributions: the distribution of charged particle multiplicity in the jets, $n^{\rm ch.}_{\rm gluon}$, and the charged particle fragmentation functions, $1/N\,({\rm d}n^{\rm ch.}_{\rm gluon}/{\rm d}x^*_E)$. We find that the results of the jet boost algorithm for the multiplicity distribution are in close correspondence to those of the gg hemispheres for jet energies $E^*_{\rm g}$ larger than about 5 GeV. For the fragmentation functions, the results of the two methods agree to good precision for $E^*_{\rm g} \gtrsim 14$ GeV.

We use the jet boost algorithm to extract measurements of the unbiased gluon jet multiplicity distribution for seven intervals of energy between 5.25 and 17.72 GeV. These are the first measurements of the $n^{\rm ch.}_{\rm gluon}$ distribution in this energy range. The distributions are analyzed to determine their means $\langle n^{\rm ch.}_{\rm gluon}\rangle$ and first two non-trivial factorial moments $F_{2,\,\rm gluon}$ and $F_{3,\,\rm gluon}$. The factorial moments are strongly correlated with the dispersion and skew of the multiplicity distribution and thus characterize its shape.

In conjunction with our previous results for unbiased gluon jet multiplicity at 40.1 GeV [7]–[9], we test two QCD analytic expressions for the energy evolution of $\langle n^{\rm ch.}_{\rm gluon}\rangle$, $F_{2,\,\rm gluon}$ and $F_{3,\,\rm gluon}$: one based on the next-to-next-to-next-to-leading order (3NLO) perturbative approximation of QCD [35, 36] and the other [40, 41] utilizing a fixed value of the strong coupling strength, α_S. The 3NLO expression takes into account the running nature of the coupling strength while the fixed α_S expression more accurately incorporates higher order effects such as energy conservation. To avoid the introduction of model dependent hadronization correction factors, the parton level analytic results are compared directly to the hadron level measurements.

The 3NLO expression for $\langle n^{\rm ch.}_{\rm gluon}\rangle$ is found to provide a good description of the data using a value of the QCD scale parameter $\Lambda = 0.296 \pm 0.037\,({\rm stat.} + {\rm syst.})$ GeV, much more similar to the corresponding result for quark jets, $\Lambda = 0.190 \pm 0.032\,({\rm stat})$ GeV [12], than found in previous studies. Our results therefore provide a much improved demonstration of the consistency of the QCD expressions for gluon and quark jet multiplicity. These results are found using $n_F = 5$, with n_F the number of active quark flavors. Very similar descriptions of the data are found using $n_F =$ 3 or 4. Note that these Λ values are not defined in the context of a particular renormalization scheme and so do not correspond e.g. to $\Lambda_{\overline{\rm MS}}$. The 3NLO expressions are found to provide a

reasonable description of the energy evolution of the $F_{2,\,\mathrm{gluon}}$ and $F_{3,\,\mathrm{gluon}}$ data between about 14 and 40 GeV, using values of Λ which are globally similar to that found from the fit to the $\langle n^{\mathrm{ch.}}_{\mathrm{gluon}} \rangle$ data. The fitted 3NLO curves lie below the $F_{2,\,\mathrm{gluon}}$ and $F_{3,\,\mathrm{gluon}}$ measurements at smaller energies, however. These discrepancies at low energies may be a consequence of hadronization effects, which are predicted to be significant for the $F_{2,\,\mathrm{gluon}}$ and $F_{3,\,\mathrm{gluon}}$ distributions. The fixed α_S expressions are found to be in general agreement with the $\langle n^{\mathrm{ch.}}_{\mathrm{gluon}} \rangle$ data, and also with the $F_{2,\,\mathrm{gluon}}$ data within fairly large theoretical uncertainties. The fixed α_S result for $F_{3,\,\mathrm{gluon}}$ lies above the data except for $E^*_{\mathrm{g}} \approx 40$ GeV.

We also examine the ratio of the gluon to quark jet mean charged particle multiplicities, $r_{\mathrm{g/q}}$, and the corresponding ratios for F_2 and F_3. We find that a numerical solution [47] of the QCD evolution equations for particle multiplicity provides a good description of the $r_{\mathrm{g/q}}$ data, while the 3NLO and fixed α_S calculations with their fitted values of Λ from the $\langle n^{\mathrm{ch.}}_{\mathrm{gluon}} \rangle$ data are 15–20% too high. This suggests that energy conservation and phase space limits, which are more properly incorporated into the numerical solution than into the analytic results, are important considerations for the accurate description of this quantity.

We measure the fragmentation function of unbiased gluon jets at 14.24 and 17.72 GeV. In conjunction with our previous measurements of unbiased gluon and quark jet fragmentation functions at 40.1 and 45.6 GeV, respectively, we fit these data using the DGLAP evolution equations at next-to-leading-order in the $\overline{\mathrm{MS}}$ scheme. This fit yields a result for the strong interaction coupling strength $\alpha_S\,(m_{\mathrm{Z}}) = 0.128 \pm 0.008\,(\mathrm{stat.}) \pm 0.015\,(\mathrm{syst.})$, consistent with the world average. While this result is not competitive in precision with other measurements of α_S, it does provide a unique consistency test of QCD.

11 Acknowledgments

We thank Igor Dremin, Patrik Edén and Bryan Webber for helpful comments and discussions.

We particularly wish to thank the SL Division for the efficient operation of the LEP accelerator at all energies and for their close cooperation with our experimental group. In addition to the support staff at our own institutions we are pleased to acknowledge the
Department of Energy, USA,
National Science Foundation, USA,
Particle Physics and Astronomy Research Council, UK,
Natural Sciences and Engineering Research Council, Canada,
Israel Science Foundation, administered by the Israel Academy of Science and Humanities,
Benoziyo Center for High Energy Physics,
Japanese Ministry of Education, Culture, Sports, Science and Technology (MEXT) and a grant under the MEXT International Science Research Program,
Japanese Society for the Promotion of Science (JSPS),
German Israeli Bi-national Science Foundation (GIF),
Bundesministerium für Bildung und Forschung, Germany,
National Research Council of Canada,
Hungarian Foundation for Scientific Research, OTKA T-038240, and T-042864,
The NWO/NATO Fund for Scientific Research, the Netherlands.

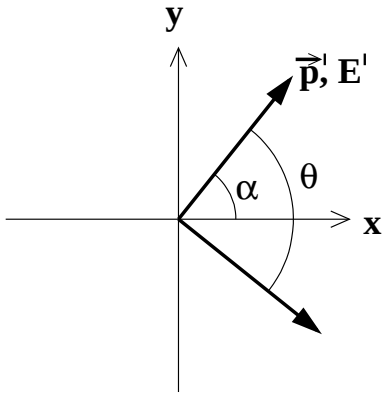

Figure 11: Schematic illustration of a two-jet system.

A Appendix: boost algebra

A.1 Boost to the back-to-back frame of a dipole

Consider a massless jet with energy E' and 3-momentum of magnitude p'. The jet lies in the x–y plane and makes angles θ and α with respect to another massless jet and the x axis, respectively (see Fig. 11). We wish to boost the event to a Lorentz frame in which the jet points along the y axis. The energy and momentum of the jet in the boosted frame are E^* and p^*. A boost along the x axis yields the condition

$$p_x^* = \gamma\,(p'_x - \beta\,E') = 0 \quad , \tag{9}$$

with $\gamma = 1/\sqrt{1-\beta^2}$ and $\beta = v$, where v is the relative speed between the boosted and original frames (note that the speed of light c is set to unity). Since $p'_x = p'\cos\alpha$ and $p' = E'$, eq. (9) yields $\beta = \cos\alpha$. The energy of the jet in the boosted frame is

$$E^* = \gamma\,(E' - \beta\,p'_x) = E'\,\sin\alpha \quad . \tag{10}$$

If the x axis corresponds to the bisector of the two jets, so that $\alpha = \theta/2$, then the same boost brings the other massless jet to the $-y$ direction so that the boosted frame corresponds to a frame in which the two jets are back-to-back. Then $\beta = \cos(\theta/2)$ and $E^* = E'\,\sin(\theta/2)$.

A.2 Boost from the c.m. frame to the symmetric frame of a three-jet $q\overline{q}g$ event

In the c.m. frame of a three-jet $q\overline{q}g$ event we define

$$x_i \equiv \frac{2\,E_i}{\sqrt{s}} \qquad i = \mathrm{q}, \bar{\mathrm{q}}, \mathrm{g} \quad , \tag{11}$$

with E_i the energy of jet i. x'_i is the corresponding quantity in the boosted reference frame for which the event is symmetric, i.e. the frame in which the angle between the gluon jet and the

quark jet is the same as the angle between the gluon jet and the antiquark jet, $\theta'_{\rm qg} = \theta'_{\bar{\rm q}{\rm g}} \equiv \theta'$ (cf. Fig. 2a for which $\theta' = \theta = 2\alpha$).

Under the assumption the jets are massless, it is straightforward to show in the c.m. frame that

$$s_{ij} = s\,(1 - x_k) \quad , \tag{12}$$

where $s_{ij} = (p_i + p_j)^2$ with p_i the 4-momentum of object i, and where i, j and k are cyclic, i.e. $i = {\rm q}$ with $j = \overline{\rm q}$ means $k = {\rm g}$, etc. The virtuality scale (eq. (2)) of the gluon jet can then be written:

$$p_{\perp,\,\rm gluon} = \frac{1}{2}\sqrt{s(1 - x_{\rm q})(1 - x_{\bar{\rm q}})} \quad . \tag{13}$$

Setting $p_{\perp,\,\rm gluon}$ equal to the jet energy scale $E^*_{\rm g}$ (see eq. (1)), as dictated by eq. (3), yields [13]

$$(1 - x_{\rm q})(1 - x_{\bar{\rm q}}) = (x'_{\rm g})^2 \sin^2 \frac{\theta'}{2} \quad . \tag{14}$$

We can also express s_{ij} using the angle between partons i and j, θ_{ij}:

$$s_{ij} = 4E_iE_j \sin^2 \frac{\theta_{ij}}{2} \quad . \tag{15}$$

This latter expression, unlike eq. (12), is valid in any frame. Evaluating eq. (15) in the symmetric frame and equating it to eq. (12) yields

$$1 - x_k = x'_i x'_j \sin^2 \frac{\theta'_{ij}}{2} \quad , \tag{16}$$

which leads to the following expression:

$$\frac{(1 - x_{\rm q})(1 - x_{\bar{\rm q}})}{1 - x_{\rm g}} = x'^2_{\rm g} \frac{\sin^2\,(\theta'_{\rm qg}/2) \sin^2\,(\theta'_{\bar{\rm q}{\rm g}}/2)}{\sin^2\,(\theta'_{\rm q\bar{q}}/2)} \quad . \tag{17}$$

Since $\theta'_{\rm qg} = \theta'_{\bar{\rm q}{\rm g}} = \theta'$ in the symmetric frame, then $\theta'_{\rm q\bar{q}} = 2\pi - 2\theta'$, so that $\sin\,(\theta'_{\rm q\bar{q}}/2) = 2\sin\,(\theta'/2)\cos\,(\theta'/2)$. Inserting these results into eq. (17) yields [13]

$$\frac{(1 - x_{\rm q})(1 - x_{\bar{\rm q}})}{1 - x_{\rm g}} = \frac{x'^2_{\rm g}}{4} \frac{\sin^2\,(\theta'/2)}{\cos^2\,(\theta'/2)} \quad . \tag{18}$$

The expression for the angle θ' [13] is obtained by combining eqs. (14) and (18):

$$\cos^2 \frac{\theta'}{2} = \frac{1 - x_{\rm g}}{4} \quad . \tag{19}$$

When inserted into eq. (14), this yields the expression for the gluon jet energy in the symmetric frame:

$$x'_{\rm g} = \sqrt{\frac{4(1 - x_{\rm q})(1 - x_{\bar{\rm q}})}{3 + x_{\rm g}}} \quad . \tag{20}$$

Similarly, using eq. (16) to derive expressions analogous to eq. (17) for $(1-x_{\rm q})(1-x_{\rm g})/(1-x_{\bar{\rm q}})$ and $(1-x_{\bar{\rm q}})(1-x_{\rm g})/(1-x_{\rm q})$ yields the results for the quark and antiquark energies in the symmetric frame:

$$x'_{\rm q} = \frac{x'_{\rm g}}{1-x_{\rm q}} \quad , \quad x'_{\bar{\rm q}} = \frac{x'_{\rm g}}{1-x_{\bar{\rm q}}} \quad . \tag{21}$$

Consider the c.m. frame of the event to be described by a Cartesian coordinate system with the z axis along the gluon jet direction and the three-jet event in the y–z plane. The scaled three momenta of the jets are then

$$2\,\vec{p}_{\rm g}/E_{\rm c.m.} = (0,0,x_{\rm g}) \tag{22}$$

$$2\,\vec{p}_{\rm q}/E_{\rm c.m.} = (0,x_{{\rm q},y},x_{{\rm q},z}) \tag{23}$$

$$2\,\vec{p}_{\bar{\rm q}}/E_{\rm c.m.} = (0,-x_{{\rm q},y},x_{\bar{\rm q},z}) \quad . \tag{24}$$

with $|\vec{p}_i| = E_i$ such that $x_{i,y}$ is the component of scaled momentum in the y direction, etc. Since we boost from the c.m. frame, the scaled energy in the symmetric frame is

$$x'_{\rm q} + x'_{\rm g} + x'_{\bar{\rm q}} = \gamma(x_{\rm q} + x_{\rm g} + x_{\bar{\rm q}}) = 2\gamma \quad , \tag{25}$$

where $\gamma = 1/\sqrt{1-\beta_y^2-\beta_z^2}$, with β_y and β_z the Lorentz boost factors along the y and z directions. Knowing all the x_i (measured), x'_i (from eqs. (20) and (21)) and γ (from eq. (25)), the transformation equations

$$x'_{\rm g} = \gamma(x_{\rm g} + \beta_z x_{\rm g}) \tag{26}$$

$$x'_{\rm q} = \gamma(x_{\rm q} + \beta_z x_{{\rm q},z} + \beta_y x_{{\rm q},y}) \tag{27}$$

can be solved to find the boost factors β_z and β_y. With the Lorentz boost factors defined, all the particles in the event can then be boosted to the symmetric event frame to define the unbiased gluon jets in the manner explained in Sect. 2.

References

[1] TASSO Collab., R. Brandelik et al., Phys. Lett. B **86** (1979) 243;
MARK-J Collab., D.P. Barber et al., Phys. Rev. Lett **43** (1979) 830;
PLUTO Collab., C. Berger et al., Phys. Lett. B **86** (1979) 418;
JADE Collab., W. Bartel et al., Phys. Lett. B **91** (1980) 142.

[2] TASSO Collab., R. Brandelik et al., Phys. Lett. B **97** (1980) 453;
PLUTO Collab., C. Berger et al., Phys. Lett. B **97** (1980) 459.

[3] S. Catani et al., Phys. Lett. B **269** (1991) 432.

[4] J.E. Huth et al., *Research Directions for the Decade*, Snowmass (1990), p. 134, ed. E.L. Berger (World Scientific, Singapore);
CDF Collab., F. Abe et al., Phys. Rev. D **45** (1992) 1448.

[5] CLEO Collab., M.S. Alam et al., Phys. Rev. D **46** (1992) 4822.

[6] CLEO Collab., M.S. Alam et al., Phys. Rev. D **56** (1997) 17.

[7] OPAL Collab., G. Alexander et al., Phys. Lett. B **388** (1996) 659.

[8] OPAL Collab., K. Ackerstaff et al., Eur. Phys. J. C **1** (1998) 479.

[9] OPAL Collab., G. Abbiendi et al., Eur. Phys. J. C **11** (1999) 217.

[10] J.W. Gary, Phys. Rev. D **49** (1994) 4503.

[11] P. Edén, G. Gustafson and V.A. Khoze, Eur. Phys. J. C **11** (1999) 345.

[12] OPAL Collab., G. Abbiendi et al., Eur. Phys. J. C **23** (2002) 597.

[13] P. Edén and G. Gustafson, JHEP **9809** (1998) 015.

[14] G. Gustafson, Phys. Lett. B **75** (1986) 453;
G. Gustafson and U. Pettersson, Nucl. Phys. B **306** (1988) 746;
B. Andersson, G. Gustafson and L. Lönnblad, Nucl. Phys. B **339** (1990) 393.

[15] Yu.L. Dokshitzer et al., JHEP **9708** (1997) 001.

[16] T. Sjöstrand, Comp. Phys. Comm. **28** (1983) 229.

[17] OPAL Collab., K. Ahmet et al., Nucl. Instr. and Meth. A **305** (1991) 275.

[18] P.P. Allport et al., Nucl. Instr. and Meth. A **346** (1994) 476.

[19] OPAL Collab., G. Alexander et al., Z. Phys. C **52** (1991) 175.

[20] OPAL Collab., K. Ackerstaff et al., Eur. Phys. J. C **2** (1998) 213;
OPAL Collab., G. Abbiendi et al., Eur. Phys. J. C **12** (2000) 567.

[21] OPAL Collab., M.Z. Akrawy et al., Phys. Lett. B **261** (1991) 334.

[22] OPAL Collab., R. Akers et al., Z. Phys. C **68** (1995) 179.

[23] Yu.L. Dokshitzer, V.A. Khoze and S.I. Troyan, Sov. J. Nucl. Phys. **47** (1988) 881.

[24] Ya.I. Azimov et al., Phys. Lett. B **165** (1985) 147;
DELPHI Collab., P. Abreu et al., Phys. Lett. B **449** (1999) 383;
ALEPH Collab., R. Barate et al., Z. Phys. C **76** (1997) 191.

[25] G. Corcella et al., JHEP **0101** (2001) 010.

[26] J. Allison et al., Nucl. Instr. and Meth. A **317** (1992) 47.

[27] OPAL Collab., G. Abbiendi et al., CERN-EP-2003-031.

[28] OPAL Collab., G. Alexander et al., Z. Phys. C **69** (1996) 543.

[29] A. Bialas and R. Peschanski, Nucl. Phys. B **273** (1986) 703.

[30] E.A. de Wolf, I.M. Dremin and W. Kittel, Phys. Rep. **270** (1996) 1.

[31] JADE Collab., W. Bartel et al., Z. Phys. C **33** (1986) 23.

[32] OPAL Collab., M.Z. Akrawy et al., Z. Phys. C **47** (1990) 505.

[33] L. Lönnblad, Comp. Phys. Comm. **71** (1992) 15.

[34] T. Sjöstrand, Comp. Phys. Comm. **82** (1994) 74.

[35] I.M. Dremin and J.W. Gary, Phys. Lett. B **459** (1999) 341.

[36] I.M. Dremin, C.S. Lam and V.A. Nechitailo, Phys. Rev. D **61** (2000) 074020.

[37] W.A. Bardeen et al., Phys. Rev. D **18** (1978) 3998.

[38] I.M. Dremin and J.W. Gary, Phys. Rep. **349** (2001) 301.

[39] Review of Particle Properties, K. Hagiwara et al., Phys. Rev. D **66**, (2002) 010001.

[40] I.M. Dremin and R.C. Hwa, Phys. Lett. B **324** (1994) 477.

[41] I.M. Dremin and R.C. Hwa, Phys. Rev. D **49** (1994) 5805.

[42] ARGUS Collab., H. Albrecht et al., Z. Phys. C **54** (1992) 13.

[43] JADE Collab., W. Bartel et al., Z. Phys. C **20** (1983) 187.

[44] HRS Collab., M. Derrick et al., Phys. Rev. D **34** (1986) 3304.

[45] TASSO Collab., W. Braunschweig et al., Z. Phys. C **45** (1989) 193.

[46] A. Capella et al., Phys. Rev. D **61** (2000) 074009.

[47] S. Lupia and W. Ochs, Phys. Lett. B **418** (1998) 214.

[48] P. Edén, Eur. Phys. J. C **19** (2001) 493.

[49] V.N. Gribov and L.N. Lipatov, Sov. J. Nucl. Phys. **15** (1972) 438; Ibid 675;
G. Altarelli and G. Parisi, Nucl. Phys. B **126** (1977) 298;
Yu.L. Dokshitzer, Sov. Phys. JETP **46** (1977) 641.

[50] OPAL Collab., K. Ackerstaff et al., Eur. Phys. J. C **7** (1999) 369.

[51] DELPHI Collab., P. Abreu et al., Eur. Phys. J. C **13** (2000) 573.

[52] Bryan Webber, private communication.

[53] P. Nason and B.R. Webber, Nucl. Phys. B **421** (1994) 473, Erratum, Ibid. **480** (1996) 755.